NTNU

Norwegian University of
Science and Technology

Reliability Analysis of Reinforced Concrete using Non-Linear Finite Element Analysis

Noman Afzal

Mats Gruber Bech Bjerva

Erlend Knudsen Henriksen

Guro Lindgren

Civil and Environmental Engineering

Submission date: June 2016

Supervisor: Max Hendriks, KT

Co-supervisor: Jochen Köhler, KT

Morten Engen, KT

Norwegian University of Science and Technology

Department of Structural Engineering

Department of Structural Engineering
Faculty of Engineering Science and Technology
NTNU- Norwegian University of Science and Technology

ACCESSIBILITY

MASTER THESIS 2016

SUBJECT AREA: Computational Mechanics	DATE: 10.06.2016	NO. OF PAGES: 112

TITLE:

Reliability Analysis of Reinforced Concrete using Non-Linear Finite Element Analysis

Pålitelighetsanalyse av armerte betongkonstruksjoner ved bruk av ikke-lineære elementanalyser

BY:

Noman Afzal
Mats Gruber Bech Bjerva
Erlend Knudsen Henriksen
Guro Lindgren

SUMMARY:
The purpose of the thesis is to investigate methods that may be used for assessing the reliability in large concrete structures in combination with non-linear finite element analyses (NLFEA).
Reliability methods are applied to a simple beam with various lengths, and evaluated with respect to applicability, accuracy and feasibility. The reliability is assessed by a response surface method in combination with a first order reliability method (RSM-FORM), and a small-sample Monte Carlo type using Latin hypercube sampling with curve fitting to a normal distribution (LHS-fit). For greater insight, these methods are investigated using both NLFEA and analytic limit state function evaluations (LSFE). Analytic Monte Carlo simulations are used as benchmarks. For very strong or weak material parameters, NLFEA yield inconsistent results.
Only two stochastic variables are introduced, namely the concrete in-situ compressive strength and steel yield strength. Thus, only material uncertainties are implemented in the reliability assessments. Since load effects are treated deterministically, this study only regards reliability of the resistance.
In the region where NLFEA is consistent and when only bending failure mode is prevalent, results from NLFEA RSM-FORM yield quite similar results compared to the benchmarks. Similarly, NLFEA LHS-fit provides decent, conservative results although less accurate than RSM-FORM. Analytic results show two important findings: (1) RSM-FORM accuracy decreases with two failure modes, and (2) the choice of distribution seems important for LHS-fit, however an optimal choice may still not provide as accurate results as RSM-FORM.
RSM-FORM shows promising results for a simple beam with one failure mode. However, for large concrete structures with several failure modes, this method might struggle to create an accurate response surface. This is further impeded by the difficulties in producing consistent NLFEA response. In terms of feasibility, RSM-FORM normally requires 10-25 LSFEs for one reliability assessment, while LHS-fit with 50 LSFEs provide the full picture of the structural reliability. LHS-fit is not as accurate as RSM-FORM, however, it is simpler to grasp and results show that it provides reasonable accuracy for preliminary reliability assessments.

RESPONSIBLE TEACHER: Max Hendriks

SUPERVISOR(S): Max Hendriks, Morten Engen, Jochen Köhler

CARRIED OUT AT: Department of Structural Engineering

NTNU
Faculty of Engineering Science
and Technology
Department of Structural Engineering

MASTER THESIS 2016

for

Noman Afzal, Mats Bjerva, Erlend Henriksen and Guro Lindgren

Large concrete shell structures like dams and offshore oil and gas platforms are normally designed using global linear finite element analyses and specially developed post-processing software. This method allows us to use the principle of superpositioning, which is necessary in order to design for the possible large number of load combinations. In order to achieve this, reinforced concrete is treated as a linear elastic material. This design procedure enables engineers to verify the reliability of a reinforced concrete structure.

Cracking of concrete and yielding of reinforcement results in a non-linear behavior, and in order to capture the true structural behavior, non-linear finite element analyses should be performed. In such analyses, all sections contribute to the global capacity of the structure. The capacity control should thus be based on a global resistance method in contrast to the local control on sectional level which is most commonly used. Global resistance methods have been developed and demonstrated for simple structures with simple arrangements, but the extension to large structures as mentioned in the introduction is still not fully explored.

The question becomes: Can non-linear finite element analyses be used for reliability purposes?

Preface

This MSc thesis is written for the Department of Structural Engineering at NTNU - Norwegian University of Science and Technology, in Trondheim.

The thesis is conducted as a collaboration between Noman Afzal, Mats Bjerva, Erlend Henriksen and Guro Lindgren. We decided to work in a group of four because we felt we could dig deeper into the subject. The study was performed using MATLAB and Python, as well as the non-linear finite element program Diana. Many months were spent developing scripts for the analyses. The report was written in LaTeX.

During the study, knowledge has been gained in regards to how reliability of concrete structures is assessed for practical engineering. Hopefully, this thesis enlightens some aspects of how reliability of large concrete structures may be performed using non-linear finite element method.

Gratitude is extended towards supervisor Professor Max Hendriks and co-supervisor PhD candidate Morten Engen at Multiconsult for invaluable help. Their guidance and motivation, sharing of knowledge and hours of discussion was invaluable to this team. A special thanks to co-supervisor Associate Professor Jochen Köhler for valuable discussion and insight into the world of reliability.

Thanks are also extended to Professor Jan Arve Øverli for supplying Diana and *fib* Bulletin No. 2.

Abstract

The purpose of the thesis is to investigate methods that may be used for assessing the reliability in large concrete structures in combination with non-linear finite element analyses (NLFEA).

Reliability methods are applied to a simple beam with various lengths, and evaluated with respect to applicability, accuracy and feasibility. The reliability is assessed by a response surface method in combination with a first order reliability method (RSM-FORM), and a small-sample Monte Carlo type using Latin hypercube sampling with curve fitting to a normal distribution (LHS-fit). For greater insight, these methods are investigated using both NLFEA and analytic limit state function evaluations (LSFE). Analytic Monte Carlo simulations are used as benchmarks. For very strong or weak material parameters, NLFEA yield inconsistent results. Only two stochastic variables are introduced, namely the concrete in-situ compressive strength and the steel yield strength. Thus, only material uncertainties are implemented in the reliability assessments. Since load effects are treated deterministically, this study only regards reliability of the resistance.

In the region where NLFEA is consistent and when only bending failure mode is prevalent, results from NLFEA RSM-FORM yield quite similar results compared to the benchmarks. Similarly, NLFEA LHS-fit provides decent, conservative results although less accurate than RSM-FORM. Analytic results show two important findings: (1) RSM-FORM accuracy decreases with two failure modes, and (2) the choice of distribution seems important for LHS-fit, however an optimal choice may still not provide as accurate results as RSM-FORM.

RSM-FORM shows promising results for a simple beam with one failure mode. However, for large concrete structures with several failure modes, this method might struggle to create an accurate response surface. This is further impeded by the difficulties in producing consistent NLFEA response. In terms of feasibility, RSM-FORM normally requires 10-25 LSFEs for one reliability assessment, while LHS-fit with 50 LSFEs provide the full picture of the structural reliability. LHS-fit is not as accurate as RSM-FORM, however, it is simpler to grasp and results show that it provides reasonable accuracy for preliminary reliability assessments.

The literature provides a variety of optimizations and improvements on the methods, which might increase their applicability for large scale reliability assessments. Results herein are promising, and should be further investigated on more complex models using improved RSMs found in the literature.

Sammendrag

Formålet med masteroppgaven er å se nærmere på hvordan ikke-lineære elementanalyser kan brukes sammen med pålitelighetsmetoder for å undersøke påliteligheten til store betongkonstruksjoner.

Hovedsakelig to pålitelighetsmetoder er blitt brukt på en fritt opplagt bjelke med forskjellige lengder og vurdert etter anvendbarhet, nøyaktighet og gjennomførbarhet. Metodene er *response surface method* i kombinasjon med *first order reliability method* (RSM-FORM), og en *small-sample Monte Carlo* sammen med *Latin hypercube sampling* og kurvetilpasning (LHS-fit). For større innsikt i metodene, benyttes både ikke-lineære elementanalyser og analytiske funksjoner. Siden de analytiske funksjonene gir en respons som er ganske lik den fra de ikke-lineære analysene, benyttes Monte Carlo simuleringer med analytiske formler som et referansenivå. Resultater fra ikke-lineære analyser er imidlertid unøyaktige for høye- eller lave materialparametere.

To stokastiske variabler er inkludert, in-situ betong trykkfasthet og flytespenning i stål. Det betyr at bare materialusikkerheter er implementert i pålitelighetsanalysene. Lasten er ikke modellert som en stokastisk variabel, hvilket betyr at pålitelighetsanalysene bare vektlegger kapasiteten.

Resultater for RSM-FORM fra de ikke-lineære analysene er ganske like referansenivået dersom det kun er én opptredende bruddmode. Resultatene for LHS-fit fra de ikke-lineære analysene viser at metoden er konservativ, men samtidig mer unøyaktig enn RSM-FORM. Analytiske resultater viser to interessante funn: (1) To opptredende bruddmoder kan påvirke nøyaktigheten til RSM-FORM, og (2) kurvetilpasningen kan påvirke LHS-fit nøyaktigheten. Videre må det presiseres at en optimal kurvetilpasning vil trolig fortsatt

ikke gi nøyaktighet på nivå med RSM-FORM.

RSM-FORM viser lovende resultater for en fritt opplagt bjelke med én bruddmode. For større betongkonstruksjoner med flere, og mer komplekse bruddmoder, kan metoden få problemer med å lage en nøyaktig responsflate. Dette forsterkes ytterligere grunnet vanskelighetene med å lage gode modeller for ikke-lineære analyser av store konstruksjoner. Med hensyn til gjennomførbarheten trenger RSM-FORM vanligvis mellom 10-25 analyser for én pålitelighetsanalyse, mens LHS-fit krever bare 50 analyser for å dekke hele pålitelighetsområdet. LHS-fit er ikke like nøyaktig som RSM-FORM, men er imidlertid enklere å bruke og gir gode nok resultater til at metoden kan benyttes som et grovt første overslag.

Contents

List of Figures

List of Tables

Lists with abbreviations and symbols

Abbreviations

CL12I	3+3 noded interface element in Diana
CSD strain failure	Concrete strength-dependent strain failure
FE	Finite element
FEA	Finite element analysis/analyses
FORM	First order reliability method
JCSS	Joint Committee on Structural Safety
LFEA	Linear finite element analysis/analyses
LHS	Latin hypercube Sampling
LHS-count	LHS using counting to asses reliability
LHS-fit	LHS using fitting to assess reliability
LSF	Limit state function
LSFE	Limit state function evaluation
NLFEA	Nonlinear finite element analysis/analyses
PDF	Probability density function
RS	Response surface
RSM	Response surface method
RSM-FORM	Response surface method with first order reliability method
SORM	Second order reliability method
Q8	Eight-noded serendipity element

Latin lower case letters

b	Cross-sectional width
b_w	Minimum cross-sectional width
c	Reinforcement cover
d	Effective depth
f	f-factor
f_c	Concrete strength
$f_{c,situ}$	Concrete in-situ compressive strength
f_{ck}	Characteristic concrete compressive strength
$f_{ck,situ}$	Characteristic concrete in-situ compressive strength
$f_{ck,situ,actual}$	Actual characteristic concrete in-situ compressive strength
$f_{ck,EC2}$	Eurocode 2 characteristic concrete cylinder compressive strength
f_{cm}	Mean concrete cylinder compressive strength
$f_{cm,EC2}$	Eurocode 2 mean concrete cylinder compressive strength
$f_{cm,situ}$	Mean concrete in-situ compressive strength
f_{cmd}	Median concrete cylinder compressive strength
$f_{cmd,situ}$	Median concrete in-situ compressive strength
f_d	Design material parameters
f_k	Characteristic material parameters
f_{sy}	Steel yield strength
f_{su}	Steel ultimate strength
f_t	Concrete tensile strength
f_{yk}	Characteristic steel yield strength
h	Height
k	Scale factor
p_f	Probability of failure
$\mathbf{u}$	Global nodal displacement
$\mathbf{u}*$	Estimated design point coordinates in standard normal space
x_i	Parameter of variable i
$\mathbf{x}*$	Estimated design point coordinates in real space

Latin upper case letters

A_s	Longitudinal reinforcement area
$\mathbf{B}$	Strain displacement operator
C	Coefficient for shear flexure capacity
G_C	Compressive fracture energy of concrete
G_F	Tensile fracture energy of concrete
E_c	Concrete Young's modulus
E_{har}	Steel hardening modulus
E_s	Steel Young's modulus
L	Beam length
$\mathbf{K}$	Stiffness matrix
M_r	Moment resistance
N	Number of stratifications in LHS
P	Load
R	Resistance
R_d	Design resistance
R_m	Resistance with mean or modified material parameters
R_k	Resistance with characteristic material parameters
S	Load
V_i	Coefficient of variation in material i
V_r	Shear flexure resistance
V_R	Coefficient of variation for resistance
V_f	Coefficient of variation in material uncertainties
V_g	Coefficient of variation in geometric uncertainties
V_m	Coefficient of variation in modelling uncertainties
Z	N(0,1) variable

Greek letters

α_i	Influence factor of parameter i, unless stated otherwise
α_{cf}	Factor for the modified mean material strength in the global safety factor format
β	Reliability index
β_{σ}^{min}	Minimum reduction factor due to lateral cracking
γ	Safety factor
ϵ_c	Concrete strain
$\epsilon_{c,par}$	Strain for maximum concrete strength in the parabolic stress-strain model
ϵ_{cu}	Concrete ultimate strain
ϵ_{FORM}	FORM Convergence criteria
ϵ_{RSM}	RSM Convergence criteria
ϵ_{su}	Steel ultimate strain
ϵ_{sy}	Steel yield strain
η	Factor for effective compression strength
λ	Factor for effective compression zone height
μ	First moment in a distribution
ν_c	Concrete Poisson's ratio
ν_p	Platen Poisson's ratio
ξ	Factor for transforming to concrete in-situ strength
ρ	Reinforcement ratio
σ	Second moment in a distribution
$\boldsymbol{\sigma}$	Stress vector
σ_s	Reinforcement stress
ψ	Factor for transforming to concrete in-situ strength
ω	Relative factor between top-neutral axis and top-A_s

Chapter 1

Introduction

Structures and technical systems need to satisfy requirements in regards to safety and serviceability for a given period of time. Such requirements describe high-risk events like total collapse of a structure, and also events less severe such as maximum deflection or vibration requirements. In traditional design today, safety and serviceability is ensured using safety factors which account for uncertainties and reflect a desired reliability level for the design. In the design of concrete components, linear finite element analyses (LFEA) are normally conducted to find critical sections and the forces acting in those sections. Next, the design resistance and the design loads of the critical sections are calculated using safety factors. The check is then to compare the design resistance with the limit state requirements stated in the codes. This procedure using LFEA together with hand calculations and sectional checks is how most codes are utilized in the design of structural components. Although the partial factor method is quite robust, there are some drawbacks to the method. Partial factors are general and do not accurately account for the stochastic properties of the variables [35]. Local checks do not give any insight to the global safety of the structure, only whether or not the design resistance is greater than the design load for a given section. This is one motivation for trying to incorporate non-linear finite element analysis (NLFEA) in the design of components and in structural reliability assessments. A NLFEA is a global check, implying that it assesses all failure modes, and hence there is no need for separate sectional checks as with the traditional design strategy. Additionally, NLFEA provide more realistic results and accounts for force redistribution and intricate interplay between components.

When modelling a structure there is always a question of how to incorporate uncertainties. Uncertainties can be related to the modelling itself, and/or material and geometric properties. The input parameters are uncertain and should therefore be represented as stochastic variables. The aforementioned partial safety factor method is a semi-probabilistic level I method, meaning that it does not explicitly account for uncertainties. Level II and level III methods, e.g., first order reliability method (FORM) and the Monte Carlo method, respectively, are more accurate and include stochastic parameters and distribution functions in the calculation of failure probabilities. The objective of reliability assessments is to compute a failure probability for the whole system. However, finding analytic formulations of the limit state function (LSF) of a complex structure is not straightforward. Hence, NLFEA is used to evaluate the LSF due to its global nature and superior representation of real structural behavior. This is where the problem arises. Reliability methods often require repeated analyses with different input parameters. Considering that a single NLFEA is time consuming, methods like Monte Carlo that require a large number of these become unfeasible. Advances in computer science and computational mechanics has led to comprehensive research trying to find efficient ways of merging stochastic analysis with advanced finite element analysis (FEA). Common remedies are to apply sampling techniques to reduce the amount of simulations, or to create response surfaces that other reliability methods can be applied to [43].

Can NLFEA be used for reliability assessment of large concrete structures? In this study, the reliability methods are evaluated with respect to feasibility, applicability and accuracy. Feasibility regards whether the methods are viable, if it is worth the time spent making the solution strategy and post-processing. This must be done with care, since many analyses are needed and the model at hand must be applicable for a range of input parameters, and able to cope with several failure modes. A model should be able to do all this without compromising the accuracy of the solution to a large extent. In probabilistic reliability assessments using FEA, there is always an issue of feasibility vs. accuracy. For the procedures to be feasible, time spent analyzing and needs for modification should be minimized. The reliability methods investigated are meant to be performed on regular computers without aid from any advanced computers.

This study focused on reliability of a simply supported beam with a mid-span point load,

evaluated analytically and using NLFEA. The Monte Carlo method is the most accurate reliability method, but is unfeasible with NLFEA. Thus, the main objective of this paper is to use an alternative approach, by employing a response surface method (RSM) in combination with FORM (RSM-FORM). Another reliability method investigated is a small sample Monte Carlo type using Latin hypercube sampling (LHS). This method is used with either curve fitting or with simple counting to provide reliability levels, denoted LHS-fit and LHS-count, respectively. Furthermore, these methods were applied to a modified analytic LSF for comparative reasons. The performance of a partial and a global safety format according to *fib* Model Code 2010 [10] are evaluated with NLFEA. The reliability methods are summarized in Table 1.1.

Table 1.1: Summary of reliability methods

Reliability method	**Analytic**	**NLFEA**
Monte Carlo	x	
RSM-FORM	x	x
LHS-fit	x	x
LHS-count	x	

In Chapter 2, the beam configuration and its input variables are presented first. Further, the NLFEA theory and the implemented solution strategy is described. Then, the analytic method is introduced, before we delve into reliability. Within reliability, general theory is presented, as well as the following reliability methods: Monte Carlo, LHS, RSM-FORM and the safety formats, followed by a section on uncertainties. The last section in Chapter 2 presents a summary of the method for limit state function evaluations (LSFEs) applied in this study. Chapter 3 presents the results, starting with a summary of the optimization procedure of the method for NLFEA LSFEs, followed by the results from the reliability analyses of RSM-FORM and LHS. The results are discussed and compared in Chapter 4. First, the method for NLFEA LSFEs, then the discussion regarding the RSM-FORM and LHS methods, respectively. Chapter 5 presents conclusions based on the discussion, and finally Chapter 6 presents a few proposals for further study.

Chapter 2

Theory and method

First, the case configuration is presented with the beam model and its stochastic variables. There is a section on NLFEA, describing and presenting analysis procedures, discretization and meshing options. In addition, material models for modelling concrete and steel are presented. The next section includes general concepts of reliability and presents some methods to estimate reliability. Then, uncertainties of FEA and reliability are presented, along with estimations found in the literature. The last section summarizes the method for LSFEs using either NLFEA or analytic formulas.

2.1 Case configuration

In this section, the case configuration as well as the stochastic variables are presented.

2.1.1 Beam model

The analyses in this report were performed on a simply supported beam with a mid-span point load. The cross-section is shown in Figure 2.1, with height $h = 400$ mm and width $b = 200$ mm. The cover to the center of reinforcement bars was $c = 50$ mm, resulting in an effective depth $d = 350$ mm. The beam only had longitudinal reinforcement with area $A_s = 350$ mm^2.

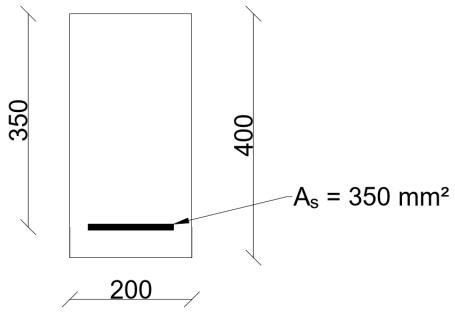

Figure 2.1: Cross-section, lengths in mm

This cross-section was applied on three different beam lengths: 1.5 m, 2.3 m and 5.0 m. These lengths were chosen to induce shear, shear-moment, and moment failure modes.

An overhang of 200 mm on each side was used on all beam lengths. Figure 2.2 illustrates the static model for the 5.0 m beam. The supports are denoted R1 and R2, and the load is denoted P1. Gravitational loads were neglected for all the beams.

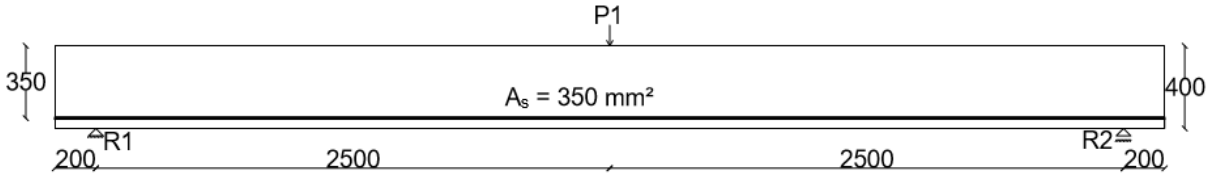

Figure 2.2: Geometry for the 5.0 m beam, lengths in mm

2.1.2 Stochastic variables

In this study, only the concrete in-situ compressive strength, $f_{c,situ}$, and steel yield strength, f_{sy}, were considered stochastic variables. All other material properties of the structure were treated deterministically related to these, and properties not related to the materials were considered deterministic. The concrete was set to C30/37, where 30 denotes the cylinder strength and 37 the cubic strength. The reinforcement steel was set to B500NC.

In the following, the concrete cylinder strength is transformed to concrete in-situ strength. Concrete cylinder strength, f_c is log-normally distributed. Its first and second moments relate to the cylinder strength by

$$f_c = e^{\mu_c + Z\sigma_c} \tag{2.1}$$

where f_c is in MPa, Z is N(0,1), and the first moment, μ_c, and the second moment, σ_c, are the mean and standard deviation of the natural logarithm of f_c, respectively. Since concrete has different behavior in a lab than in the field, concrete in-situ strength was used to better model the actual behavior. The relation between concrete cylinder and in-situ strength is collected from JCSS [22] and expressed by

$$f_{c,situ} = \xi f_c^{\psi} \tag{2.2}$$

where $f_{c,situ}$ is in MPa, ψ was set to 0.96 and ξ is a factor taking into account age at first loading, and duration of loading. ξ was set to 0.8 for loading at 28 days. Using (2.2), the concrete in-situ strength distribution was calculated from realizations of f_c, and fitted to a log-normal distribution. From this, the first and second moments of the concrete in-situ strength were calculated. These results, for a selection of concrete grades are summarized in Table 2.1.

Table 2.1: The log-normal parameters of f_c and $f_{c,situ}$ [22]

Concrete grade	**C15/19**	**C25/30**	**C35/45**	**C45/55**
μ_c	3.40	3.65	3.85	3.98
σ_c	0.192	0.164	0.123	0.096
$\mu_{c,situ}$	3.04	3.28	3.47	3.60
$\sigma_{c,situ}$	0.184	0.158	0.118	0.092

By manipulating the numbers in Table 2.1, it was found that a linear relation between the concrete cylinder and in-situ strength distribution parameters could be expressed by

$$\mu_{c,situ} = \frac{\mu_c}{1.1114} \qquad \text{and} \qquad \sigma_{c,situ} = \frac{\sigma_c}{1.0417} \tag{2.3}$$

with standard deviations of $5.2 \cdot 10^{-3}$ and $2.8 \cdot 10^{-14}$, respectively. With such small standard deviations, the relations were assumed appropriate for this study.

Note that $f_{c,situ}$ is still dependent upon the concrete grade, and Figure 2.3 shows this dependency. Here, f_{cm} is the mean cylinder strength, f_{cmd} is the median cylinder strength, $f_{cm,EC2}$ is the mean cylinder strength by Eurocode 2 [2], $f_{cm,situ}$ is the mean in-situ strength and $f_{cmd,situ}$ is the median in-situ strength of the concrete. Eurocode 2 relates the mean cylinder strength and the characteristic strength by $f_{cm,EC2} = f_{ck,EC2} + 8$ MPa.

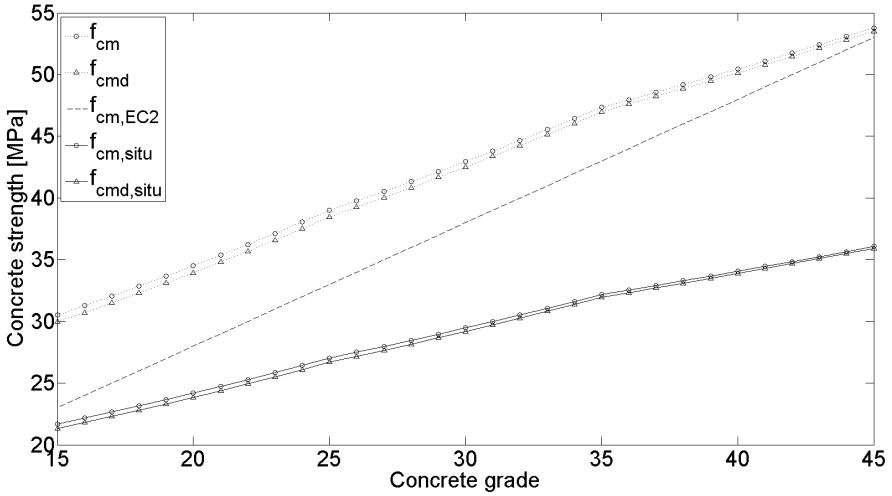

Figure 2.3: Various concrete strengths by the concrete grade

For the purpose of calculating material properties used in the NLFEA, the characteristic concrete in-situ strength was needed, $f_{ck,situ}$. A log-normal probability density function (PDF) of $f_{c,situ}$ was made with realizations of f_c by (2.2). The 5th percentile value corresponding to the actual characteristic concrete in-situ strength, $f_{ck,situ,actual}$ was then found. In order to express $f_{ck,situ}$ in the same manner as Eurocode 2, the following simplified relation was proposed:

$$f_{cmd,situ} = f_{ck,situ} + 6 \text{ MPa} \tag{2.4}$$

Figure 2.4 illustrates $f_{cmd,situ}$, $f_{ck,situ,actual}$ and $f_{ck,situ}$ with this relationship.

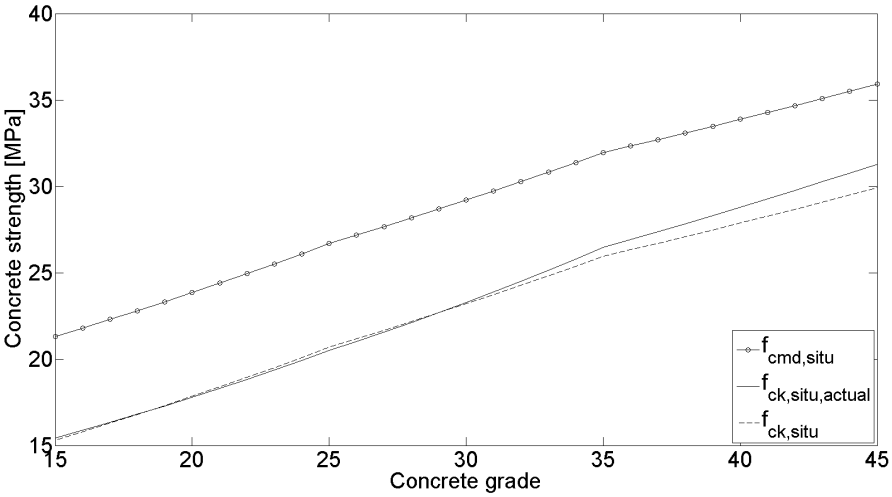

Figure 2.4: Approximation of $f_{ck,situ}$ by the concrete grade

The proposed calculation of $f_{ck,situ}$ lies close to the $f_{ck,situ,actual}$. Conservative inaccuracies occur at high concrete grades, with a maximum error of 4.4%. A non-conservative inaccuracy is located about C25/30, with 0.1% at the most.

In this study, concrete C30/37 was used and expressed by $f_{c,situ}$ with stochastic parameters logN(3.37,0.138).

For steel, the statistical properties of f_{sy} were collected from JCSS [22] in the same manner as for the concrete. Since steel is prefabricated, its strength does not change from a lab to the field, and in-situ parameters are not relevant. The standard deviation for the yield stress came from three partial variables, representing variations from mill to mill, batch to batch and within the batch itself.

$$\sigma_s = \sqrt{\sigma_{mill}^2 + \sigma_{batch}^2 + \sigma_{within}^2} \tag{2.5}$$

where $\sigma_{batch} = 22$ MPa and $\sigma_{within} = 8$ MPa. In this study, σ_{mill} was set to zero, although JCSS recommends $\sigma_{mill} = 19$ MPa. The standard deviation for steel then became $\sigma_s = 23.4$ MPa. It is worth noting that the reinforcement ultimate strength f_{su} is presented in JCSS with a larger standard deviation, although without a mean value.

Steel was assumed $\mathrm{N}(S_{nom} + 60, \sigma_s)$ where S_{nom} denotes steel grade in MPa. For B500NC this became $\mathrm{N}(560, 23.4)$.

2.2 Non-linear finite element method

When performing both LFEA and NLFEA, there are many options to consider, and the choice of these can majorly affect the output. Numerous analysis procedures, discretization and mesh options, as well as material models can be applicable. In this section, relevant theory and the options used are presented. Unless stated otherwise, options were chosen as recommended by the Guidelines for NLFEA [6]. For more in depth theory, the reader is referred to Bell [4] and Cook et al. [12].

2.2.1 General finite element method

In general, the objective of a FEA is to solve the equation

$$\mathbf{Ku} = \mathbf{R} \tag{2.6}$$

with respect to the global nodal displacements $\mathbf{u}$. $\mathbf{K}$ is the global stiffness matrix, and $\mathbf{R}$ is the global nodal forces. For a LFEA, there is a linear relation between load and displacement. In other words, $\mathbf{K}$ is constant, and $\mathbf{R}$ represents both the internal forces, $\mathbf{R_{int}}$, and external forces, $\mathbf{R_{ext}}$. There is a one-to-one relationship, and the solution is trivial. The global nodal displacements, $\mathbf{u}$, will through kinematic and constitutive relations give rise to strains, stresses, and displacements inside the elements. To assess the non-linear nature in materials, a NLFEA can be performed. Here, the stiffness, $\mathbf{K}$, and forces, $\mathbf{R}$, become a function of the displacements, $\mathbf{u}$. Then, the equilibrium equation depends on the displacement history:

$$\mathbf{K(u)u} = \mathbf{R(u)} \tag{2.7}$$

Now, the internal and external forces are not equal. Instead of defining the internal forces as a function of stiffness and displacement as in (2.6), they are now defined based on an integration of the internal stresses over the volume

$$\mathbf{R_{int}} = \int_V \mathbf{B}^T \boldsymbol{\sigma} \mathrm{d}V \tag{2.8}$$

where $\mathbf{B}$ is the strain-displacement matrix, and $\boldsymbol{\sigma}$ is the internal stress matrix [27]. Next, a residual force, $\mathbf{R_{res}}$, is defined as the difference between external and internal forces

$$\mathbf{R_{res}} = \mathbf{R_{ext}} - \mathbf{R_{int}} \tag{2.9}$$

To solve this equation, some form of analysis procedure is needed [12, 26].

2.2.2 Analysis procedure

One way to solve a non-linear problem is to use an incremental-iterative solver. There are several methods to increment the external effects e.g. load control, displacement control, or the updated normal plane arc-length method (UNP) as seen in Figure 2.5 [26].

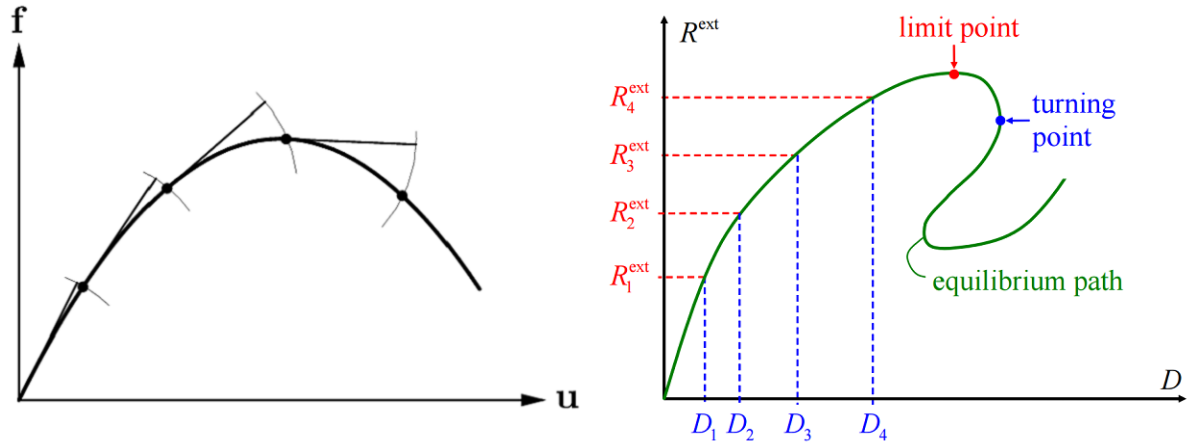

(a) Updated normal plane arc-length method [25] (b) Load and displacement control [26]

Figure 2.5: Incrementation procedures

With load control, the external effects are applied with load incrementation. A drawback with this method, is that it cannot go beyond limit points as seen in Figure 2.5b [28]. Cracking in reinforced concrete may lead to such limit points, making load control a sub-optimal incrementation technique for reinforced concrete.

Displacement control applies the external effects with displacement incrementation. It can go past limit points, but not turning points. UNP can go beyond both these points by combining both load and displacement control. UNP, as shown in Figure 2.5a, is an arc-length method where the perpendicular iterative increment is updated for every iteration. For all incrementation procedures the incrementation specification can be manual or automatic [25].

For each incremental step in a NLFEA, the residual forces are rarely zero. Without correction, this can lead to inaccurate response. To improve the solution, an iterative solver can be used to reduce the residual. The user can allow the iterative solver to stop if a convergence criterion is met, or a maximum number of iterations are reached. Examples of convergence criteria include force and energy norms. Divergence can also stop the iterative solver, and a divergence criterion is needed.

Regular Newton-Raphson (N-R) is illustrated in Figure 2.6a, and is an iterative solver where the tangent stiffness is calculated for each iteration. When concrete cracks, the

tangent of regular N-R can oscillate, leading to a non-converged step [27]. Another iterative solver is the modified N-R, illustrated in Figure 2.6b. Modified N-R uses the initial stiffness on all iterations within one incremental step. This is cheaper per iteration, but may require more iterations per incremental step for convergence. A third option is Quasi-Newton, which uses the secant stiffness.

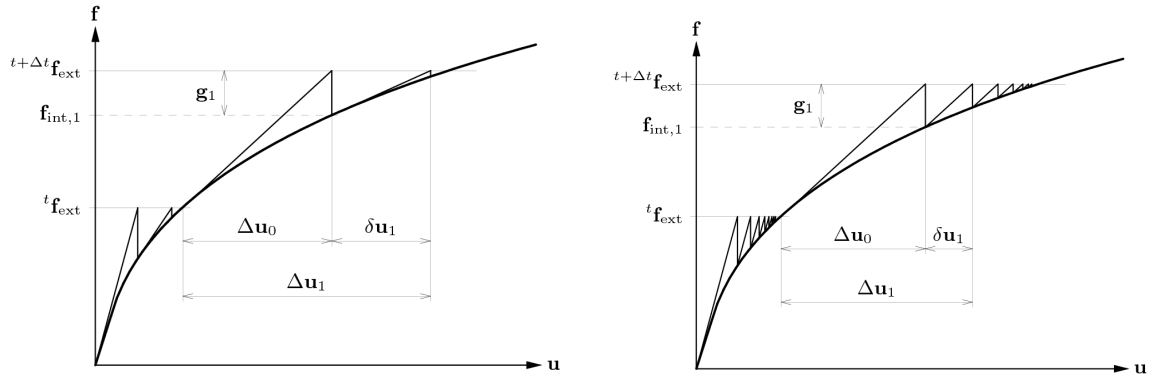

(a) Regular Newton-Raphson

(b) Modified Newton-Raphson

Figure 2.6: Newton-Raphson methods [25]

In FEA, the structure is discretized into finite elements. The choice of elements depends upon the FE formulation and the number of dimensions, and is crucial for an adequate solution. Some elements have defects that can substantially reduce the accuracy of the solution. For a 2D, non-isoparametric formulation, the Guidelines for NLFEA [6] states that the eight-noded serendipity element, Q8, provides adequate results. According to the Guidelines for NLFEA [6], the recommended maximum element size for a 2D beam is

$$\min\left(\frac{L}{50}, \frac{h}{6}\right) \tag{2.10}$$

where L is the length of the span and h is the depth of the beam. A coarse mesh may lead to inaccurate results. It is recommended to use full Gauss integration on this element, which corresponds to a 3x3 integration scheme.

Reinforcement in NLFEA can be modelled as an embedded reinforcement bar. This means that the material properties from the reinforcement is added to the mother element it lies within. The mother element and the reinforcement share some degrees of freedom. For both the mother element and the reinforcement, the strain state is found at integration points [25].

The Guidelines for NLFEA [6] also recommends that boundary constraints are modelled with the use of platens to reduce the effect of spurious high stress concentrations. This is especially a problem for fine meshes. These platens are very stiff compared to the concrete, which creates a changed stress/strain field due to friction. To overcome this, interface elements can be used to separate the element edges, making sure that no friction occurs.

In this thesis, the Q8 element with width and height $\frac{h}{6} = 66.7$ mm was used, as recommended by the Guidelines for NLFEA [6]. However, the concrete elements over the platens had a width of 75 mm. All elements were used with reduced integration which corresponds to a 2x2 integration scheme, although the Guidelines for NLFEA [6] recommends full 3x3 integration. The solution method was Sparse Cholesky using factorization and substructuring when profitable. The convergence tolerance here was set to 10^{-8}, both for solving the incremental step equilibrium and the iteration equilibrium. To apply the reference load, $P1 = 100$ kN, user specified sizes were applied with UNP using regular control type. The unloading determination was done by sign change. The iterative solver was a regular N-R procedure. This was applied with line search with a lower and upper bound of 0.1 and 1, respectively. The maximum number of searches was set to 5, the energy psi criterion was set to 0.8, and the regula falsi interval delta eta was set to 0.1. 100 iterations were allowed in each incremental step, and the analysis was set to continue even if convergence was not reached. The incremental step converged for an energy norm < 0.001 or a force norm < 0.01. The analysis would stop due to divergence for a value in either norm > 10000.

2.2.3 Material models

For a mathematical model to describe the real problem in the best way, it is important to choose a proper material model and properties for the problem at hand.

Concrete

Concrete is a highly non-linear material, and many effects need to be modeled to replicate the real behavior.

The tensile behavior of concrete includes a crack model and a stress-strain relationship. Cracking in concrete can be modelled as smeared, which makes the concrete continuous, and the stiffness matrix is only updated after cracking [25]. A smeared approach recommended by the Guidelines for NFLEA, is the total strain-based crack model, where the cracks can be considered fixed or rotating [6]. In the rotating crack model, the cracks co-rotate with the principal stress directions. Due to the rough nature of concrete, some stresses can be transferred over the cracks [39]. For the total strain-based rotating crack model, there are a variety of tensile curves to model the tensile behavior. One of these is the exponential curve [25]. As Figure 2.7 shows, this stress-strain relationship has a softening effect after the maximum tensile strength, f_t, is reached.

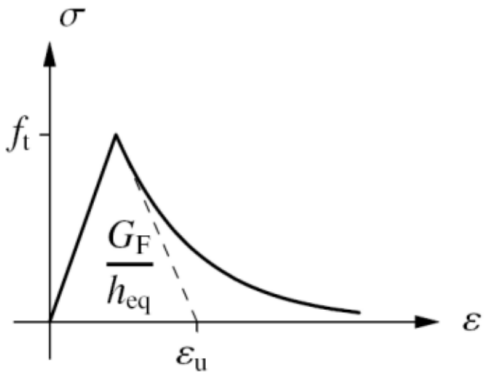

Figure 2.7: Exponential tensile stress-strain model [6]

The material parameters included in the exponential softening model are the tensile strength of concrete, f_t, the fracture energy, G_F, and Young's modulus, E_c, for the elastic region [19]. h_{eq} is an equivalent element length dependent on the mesh discretization. By the Guidelines for NLFEA [6], G_F and f_t can be calculated by

$$G_F = 73\ f_{cm}^{0.18} \qquad \text{and} \qquad f_t = 0.3\ f_{ck}^{2/3} \tag{2.11}$$

where f_{cm} is the mean concrete compressive strength and f_{ck} is the characteristic compressive strength in MPa. G_F is in Nmm/mm^2, and f_t is in MPa.

The concrete behavior in compression is complex. The Guidelines for NLFEA [6] suggests a parabolic stress-strain relationship in compression, as illustrated in Figure 2.8.

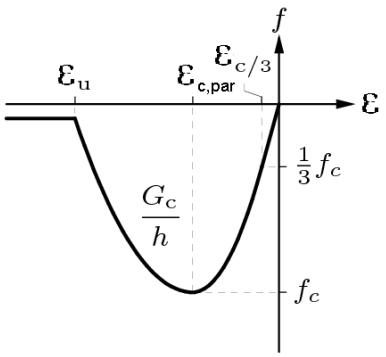

Figure 2.8: Parabolic compressive stress-strain model. Modified to our notations [25]

The parabolic model is dependent upon the compressive fracture energy, G_C, the maximum compressive strength, f_c, the Young's modulus, E_c, the strains, ϵ, and the element size, h [16, 25]. G_C is in Nmm/mm^2 and can be calculated from

$$G_C = 250\ G_F \tag{2.12}$$

Instead of a sudden decrease to zero compressive strength, the model contains a softening effect after the maximum compressive strength, f_c, is reached. The strain at maximum compressive stress, $\epsilon_{c,par}$, is defined in TNO [25] as

$$\epsilon_{c,par} = -\frac{5}{3}\frac{f_c}{E_c} \tag{2.13}$$

The maximum compressive strength of concrete depends on the multi-directional stress state. The strength increases with confined compressive stresses in the lateral directions, and decreases with tensile stresses. This can be modelled by a 1993 Selby and Vecchio model [39]. In general, the concrete has reduced compressive strength when lateral cracking occurs. One of the models for lateral cracking is model B, suggested by Vecchio and Collins [42] and is illustrated in Figure 2.9. Here, the compressive strength of the concrete, f_c, is reduced by a reduction factor, $\beta_{\sigma_{cr}}$ [25].

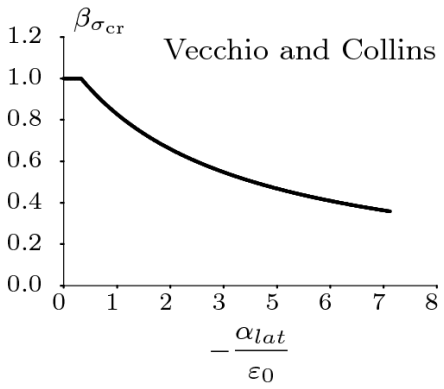

Figure 2.9: Model B suggested by Vecchio and Collins [25]

Poisson's ratio, ν_c, dictates how stresses and strains in different directions are affected by each other. For a cracked and discontinuous volume, this relationship changes, and ν_c changes with cracking. This can be modeled with a damage-based approach, where ν_c is gradually reduced to zero as cracking occurs [25]. The Guidelines for NLFEA [6] recommends the following relation to approximate E_c:

$$E_c = E_{c0} \left(\frac{f_{cm}}{10} \right)^{1/3} \tag{2.14}$$

where $E_{c0} = 21500$ MPa, and f_{cm} is in MPa.

For this report, a parabolic stress-strain model was used in compression, and an exponential stress-strain model was used in tension. The total strain-based rotating crack model was used with automatic crack bandwidth. The Vecchio and Collins 1993 model was used for reduction due to lateral cracking, with a minimum reduction factor $\beta_\sigma^{min} = 0.6$ as used by Belletti et al. [5], although the Guidelines for NLFEA recommend $\beta_\sigma^{min} = 0.4$. Poisson's ratio was modeled with a damage based reduction, and the stress confinement effect used a Selby and Vecchio model. Input material parameters were calculated based on relations from the Guidelines for NLFEA [6] and are presented in Table 2.2. f_{cm} is adapted to $f_{c,situ}$, and f_{ck} is adapted to the expression presented in (2.4).

Table 2.2: Concrete properties

Property	**Value**
Initial Poisson's ratio	$\nu_c = 0.15$
Tensile strength	$f_{ct,situ} = 0.3(f_{c,situ} - 6)^{2/3}$
Fracture energy	$G_{F,situ} = 73 f_{c,situ}^{0.18}$
Compressive fracture energy	$G_{C,situ} = 250 G_{F,situ}$
Young's modulus	$E_{c,situ} = E_{c0} \left(\frac{f_{c,situ}}{10}\right)^{1/3}$

Reinforcement steel

The material model recommended by the Guidelines for NLFEA [6] for reinforcement is rather simple compared to that of concrete. An isotropic bi-linear elasto-plastic stress-strain relationship, as illustrated in Figure 2.10, is sufficient.

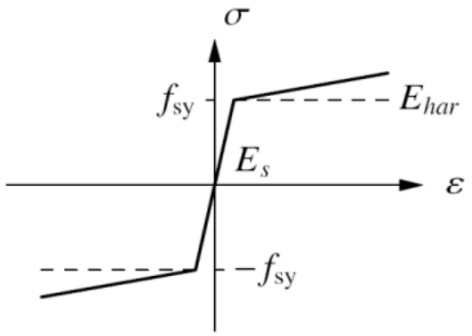

Figure 2.10: Bilinear stress-strain relationship for reinforcement [6]

This is a form of von Mises plasticity, where Hooke's law is valid for the linear part, as

$$\epsilon_{sy} = \frac{f_{sy}}{E_s} \tag{2.15}$$

where ϵ_{sy} is the yield strain, E_s is Young's modulus, and f_{sy} is the yield strength. The ultimate strain, ϵ_{su}, and ultimate strength, f_{su}, are needed to define the elasto-plastic part. The following relationship is used:

$$\epsilon_{su} = \frac{f_{su} - f_{sy}}{E_{har}} + \epsilon_{sy} \tag{2.16}$$

where E_{har} is the hardening modulus.

There are several ways to create a complete stress-strain relation for reinforcement. For a class C reinforcement, the Guidelines for NLFEA [6] provide recommendations for the ultimate and yield stress relation, $\frac{fsu}{fsy}_k$, as well as a characteristic ultimate strain limit, ϵ_{uk}:

$$1.15 \leq (\frac{f_{su}}{f_{sy}})_k \leq 1.35 \qquad \text{and} \qquad \epsilon_{uk} \geq 7\% \tag{2.17}$$

The steel parameters used in this report are summarized in Table 2.3. Note that E_{har} is not a fixed parameter, but depends upon f_{sy}, ϵ_{sy} and f_{su}. Perfect bonding between concrete and reinforcement was assumed.

Table 2.3: Reinforcement properties

Property	**Value**
Young's modulus	$E_s = 200\,000$ MPa
Ultimate strain	$\epsilon_{su} = 7.5\%$
Yield strain	$\epsilon_{sy} = \frac{f_{sy}}{E_s}$
Ultimate stress	$f_{su} = 1.25\ f_{sy}$

Platen

The platens were modeled as steel plates with a linear elastic behavior and material properties as in Table 2.4.

Table 2.4: Platen properties

Property	**Value**
Young's modulus	$E_p = 200\,000$ MPa
Poisson's ratio	$\nu_p = 0.3$

The properties for the interface elements are given in Table 2.5. These stiffnesses are collected from a benchmark experiment similar to the beam under consideration, as used by Belletti et al. [5].

Table 2.5: Interface properties

Property	**Value**
Normal stiffness	$K_n = 36\,300$ N/mm^3
Shear stiffness	$K_s = 3.63 \cdot 10^{-8}$ N/mm^3

2.3 Reliability

In a reliability assessment, the probability of failure within a lifetime of a structure is sought. Calculating failure probabilities exactly is difficult, hence many approximate methods have been developed. This is a topic highly relevant for design codes as they carry the responsibility of ensuring certain safety levels. This section presents general concepts of reliability, as well as reliability methods to estimate failure probabilities.

2.3.1 General concepts

A structure or a technical system needs to meet certain requirements in regards to safety and serviceability. These can be assessed with ultimate limit state or service limit state. Mathematically, this can be expressed as a limit state condition on the form

$$G(\mathbf{x}) > 0 \tag{2.18}$$

where $\mathbf{x}$ is the vector of random variables x_i. For a structural problem, x_i can represent properties like dimensions of components, stiffness values, loads, etc. A structure failing to meet the limit state requirements can be expressed as $G(\mathbf{x}) < 0$. The equality $G(\mathbf{x}) = 0$ is defined as the limit state function (LSF). A LSF separates the failure domain from the safe domain, and is used to express a structure's probability of failure:

$$p_f = P(G(\mathbf{x}) < 0) = \int_D f_{\mathbf{x}}(x_1, ..., x_n) dx_1 ... dx_n \tag{2.19}$$

where $f_{\mathbf{x}}(x_1, ..., x_n)$ is the joint PDF for all random variables, and D is the failure domain defined by $G(\mathbf{x}) < 0$. Computing this integral is in many ways what reliability theory is about.

In order to elucidate the methodology of reliability assessment, the method of Basler is presented using Cornell's notation [38]. A LSF of the following form is presented

$$G = R - S \tag{2.20}$$

where R represents resistance, and S denotes the load. Normally these will depend upon many variables, and are likely to be somewhat related, i.e., a thicker beam will give more resistance, but also increase the self-weight. Here, it is assumed that these two variables are independent of each other. Further, $G < 0$ physically means that the load exceeds the resistance of the system.

Schneider [38] refers to the LSF as the safety margin, M, a stochastic variable with an associated PDF that originates in the distributions of S and R. The reliability index, β, is defined in terms of the first and second moment of M. For a normally distributed variable, this will be

$$\beta = \frac{\mu_M}{\sigma_M} \tag{2.21}$$

where μ_M is the mean of the marginal distribution function and σ_M is the standard deviation. In Figure 2.11, the probability of failure is represented by the gray area in the PDF of M, and can be found from standard normal tables as $p_f = \Phi(-\beta)$. If R and S are normally distributed, so is the safety margin, and the probability of failure is exact. A more intuitive way of interpreting the reliability index is as the distance from μ_M to the unsafe region defined by $M < 0$, relative to σ_M.

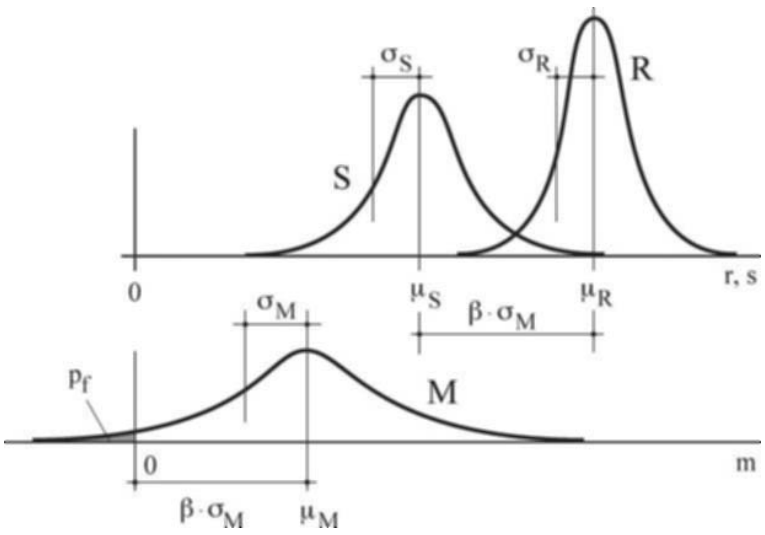

Figure 2.11: Safety margin [38]

For non-linear LSFs and other distributions of the variables, it can be advantageous to transform the variables' PDFs to N(0,1) [18, 38]. A step-by-step procedure for transforming normal and log-normal distributions to standard normal space is presented in Appendix C. Finding β can be extended to create a design condition. See Schneider [38] for details.

Influence factors, α_i, indicate how much each variable in a LSF contributes to the reliability. These can be expressed mathematically as

$$\alpha_i = \frac{\sigma_i}{\sqrt{\sum_{i=1}^{n} \sigma_i^2}} \qquad \text{and} \qquad \sum \alpha_i^2 = 1 \tag{2.22}$$

where σ_i denotes the standard deviation. In the design condition, typically partial safety factors (PSF) are used, here denoted by γ_i. These can be calculated using the influence factors, the desired reliability level and the coefficient of variation, V_i, in the following way for a normally distributed variable:

$$\gamma_i = 1 + \alpha_i \beta V_i \tag{2.23}$$

β prescribes a certain safety level for the assessment. If the desired safety level is high, this yields a low probability of failure and consequently a high PSF. α_i ensures that the PSFs for the different variables are scaled according to their relative importance. Coefficient of variation accounts for the scatter in a random variable. If a variable has a large coefficient of variation, the more uncertain are the realizations of the variable, therefore requiring a higher PSF.

Based on the problem at hand, PSFs are uniquely described through the specific α_i and V_i. This means that for every change in the case configuration, whether it is a variation in dimension or reinforcement layout, the PSFs change. However, since model codes need to be pragmatic and safe, some general values for the PSFs are carefully chosen. For a consequence class 2 and reference period of 50 years, Eurocode 0 [1] recommends a system reliability of $\beta = 3.8$. Adjusting for the influence factors of resistance and load, the target reliability is $\beta_R = \alpha_R \beta = 3.04$ for the resistance. Note that $\alpha_R = 0.8$ is not case-specific, but a general value for the dominating variable on the resistance side [1].

There are several methods proposed to assess reliability, and the methods can be categorized in three levels depending on the level of precision and complexity of the method. The categorization used in this report is by Schneider [38], Waarts [43]. Level I methods are semi-probabilistic, meaning that they do not address uncertainties of a given problem specifically, only generally through safety factors. These methods do not provide failure probabilities explicitly, but verify whether the level of reliability is sufficient. Such methods are found in structural codes like Eurocode 2 and *fib* Model Code 2010. Level II methods include the first- and second moment of the stochastic variables and can calculate β. Methods included at this level are FORM and second order reliability method (SORM) [43]. Level III assessment is a fully probabilistic analysis including accurate PDFs and human errors. These are considered most accurate in the calculation of β. Monte Carlo methods are level III methods.

2.3.2 Reliability assessment methods

In this study, different methods of assessing reliability are applied, including full probabilistic and semi-probabilistic methods, used in conjunction with NLFEA. Full probabilistic methods included in this study are a Monte Carlo method with analytic LSFs, and a small-sample Monte Carlo type using LHS with analytic and NLFEA LSFs. Furthermore, RSM-FORM is evaluated both with analytic and NLFEA LSFs. The semi-probabilistic approaches included are the global resistance factor method and the partial factor method. One LSFE is the same as performing a virtual experiment, either using NLFEA or analytically. The accuracy of the reliability methods rely on the quality of the method for LSFEs.

Monte Carlo

The intuitive and robust method of Monte Carlo is deemed the most exact way of finding failure probabilities. The idea is to do virtual experiments on random sets of the non-deterministic input values, and simply count the number of failures. Dividing the number of failures by the total number of evaluations yields the failure probability.

In the Monte Carlo method, random sampling is applied to create a set of realizations. In structural reliability, low failure probabilities are sought, which require many analyses in order to reduce statistical errors [29]. For a typical target probability of failure of a structure $p_f = 0.0001$ with a coefficient of variation $v_{p_f} = 10\%$, the number of evaluations needed to ensure appropriate accuracy is about one million [38]. The number of samples required in a Monte Carlo simulation is independent of the number of variables [43]. For structural engineering, a single NLFEA is time consuming. This combined with the number of samples required makes the Monte Carlo method infeasible. To remedy the high number of evaluations, other sampling techniques exist that demand fewer evaluations, like different variations of importance sampling [34, 36].

In this study, Monte Carlo was only used with analytic LSF. Depending on the target reliability, the number of samples was in the range 10^4 to 10^8. The sample size was chosen such that at least fifteen LSFEs failed. β was calculated by using the inverse of a normal cumulative distribution function. Three Monte Carlo simulations were performed for each load on the three beam lengths to reduce statistical errors, and the mean number of failures was chosen to calculte the resulting β.

Latin hypercube sampling

LHS was first described by Mckay et al. [29], and has later been applied in various ways in several engineering fields [13, 17, 23, 33, 35]. LHS is a sampling technique that falls within the category of stratified sampling. The key feature of LHS is the stratification of the probability distribution of each variable x_i into N equiprobable intervals, as illustrated in Figure 2.12. For each variable, one realization from each of the N intervals are chosen, either at random or systematically as the mean value or the value representing the middle of the interval. The realizations are taken from the inverse transformation of the cumulative distribution functions of the variables.

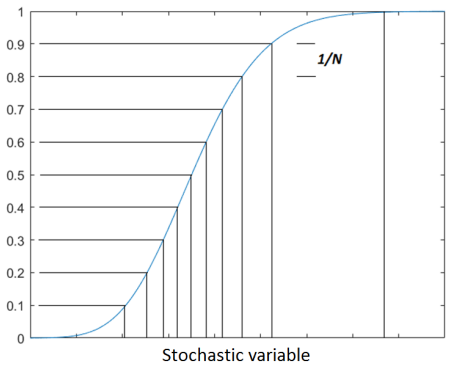

Figure 2.12: Depicting stratification into equiprobable intervals for $N = 10$

Next, the N realizations of each variable are combined through random permutations of numbers from 1 to N where each interval is only represented once. Thus, the total number of simulations is equal to the number of intervals, N. Figure 2.13 illustrates how samples are generated from two variables that are both divided into five intervals. The figure depicts how dividing the range into intervals that are only used once, reduces the risk of clustering. Analogous to this simple example with two variables and five intervals, the method is also applicable to several variables with many intervals. Further, the method can match target correlations between variables and the reader is referred to Iman and Conover [20] for more information. Although each interval is used only once, there is a risk of spurious correlation between variables as illustrated in Figure 2.14. There are various forms of LHS including spurious correlation removal techniques, importance sampling, and transformed importance LHS. See Florian [17] and Olsson et al. [33] for an overview.

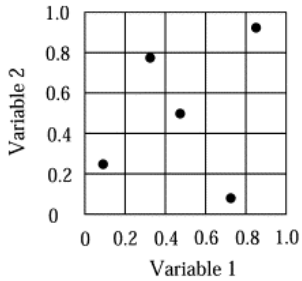

Figure 2.13: LHS applied to two variables with N=5. Extract from Olsson et al. [33]

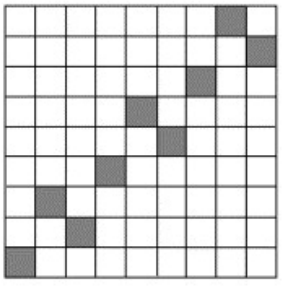

Figure 2.14: Example of spurious correlation. Extract from Olsson et al. [33]

In this study, a simple form of LHS, as it has been described in this section, was applied. Hereon LHS is written with a suffix to indicate the reliability method used, i.e., LHS-fit

denotes the reliability method where curve fitting of load capacities is used, and LHS-count denotes the method where counting the number of failures is used. Five sample sets of $N = 50$, generated from a MATLAB script written by B. Minasny [30], were analyzed using NLFEA on the 5.0 m beam. Additionally, for comparative reasons LHS-fit and LHS-count were performed on analytic LSFs for all beam lengths.

Obtaining β from LHS-fit for a resistance R_i is done using stochastic parameters from the curve fit in the following way

$$\beta = \frac{\mu - R_i}{\sigma} \tag{2.24}$$

RSM-FORM

The basic idea of a RSM is to approximate the real LSF by a polynomial based on LSFEs in selected points. Next, a reliability method, e.g. FORM, can be used to find β by linearizing the response surface (RS) polynomial. Applying a RSM in conjunction with FORM will from hereon be referred to as RSM-FORM. This is considered a level II reliability method, since it considers information about the probability distributions of the variables.

The RS polynomial can be found in many ways, Bucher and Bourgund [8] recommend to create a second order polynomial without mixed terms. This can be on the form

$$\bar{g}(\mathbf{x}) = a + \sum_{i=1}^{n} b_i x_i + \sum_{i=1}^{n} c_i x_i^2 \tag{2.25}$$

where the constants a, b_i and c_i are determined by evaluations of the LSF. The location of the sample points, x_i, are typically taken as the variable mean and varied with the product of a factor, f, and the standard deviation. This yields the following coordinates: $x_i = \mu_i$ and $x_i = \mu_i \pm f\sigma_{x_i}$. It is beneficial for the programming algorithm to transform the variables into standard normal space. Then, the sample points will be located on the origin axes with coordinates: $u_i = 0$ and $u_i = \pm f$. The f-factor, can take any value, however $f = 3.0$ is recommended, and also to keep it constant within the variables [7].

The RS in (2.25) is used to find an estimate of the design point, **u***, which corresponds to the point on the RS that is closest to the center point. The next step is to perform a second round of RSM, but now use the updated design point as the center point for

evaluations, and again vary each variable in standard normal space with $\pm f$ to find a new RS. A new center point is found, and is compared to the previous one. If these are sufficiently close, the iteration procedure has converged. Otherwise, a new RSM iteration is initiated. For a case with two stochastic variables, this is illustrated in Figure 2.15. Here three RSM iterations were performed, and each design point was optimized using FORM which will be described next. In this figure, SP represents the starting point located at the median values of the variables. The first RSM iteration yields the first design point, DP 1. Then a new RS is found from here, with a new design point, DP 2. The location of the design points were compared, and a third RSM iteration was needed. The last two design points were sufficiently close, so RSM converged.

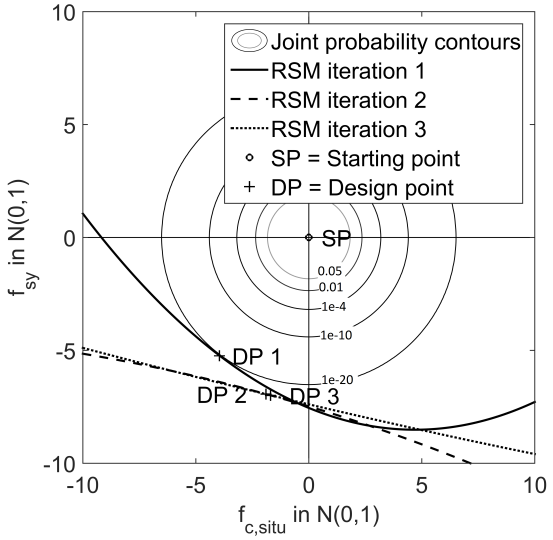

Figure 2.15: Three iterations of RSM in standard normal space

There are several reliability methods that can be used in combination with RSM. FORM is recommended in the literature [3, 8, 43]. The essence of FORM is to make a linear approximation to the RS and find **u***, which is repeated until a convergence criterion is met. In a structural reliability analysis, one is searching for the smallest distance from the design point to the origin in the standard normal space of the variables [24]. This distance corresponds to β.

FORM linearizes the RS in the design point by making a Taylor series expansion and

ignoring higher order terms [38]. This will lead to an approximate LSF of the form

$$G(\mathbf{x}) \approx a_0 + \sum_{i=1}^{n} a_i x_i \tag{2.26}$$

where a_0 and a_i are constants. The mean and standard deviation of the linearization, G, is found, and the reliability level can be found by (2.21). The influence factors of each of the variables can be found by

$$\alpha_i = \frac{\sigma_i}{\sigma_G} a_i \tag{2.27}$$

In standard normal space, the coordinate of the design point for variable i, is $u_i = \alpha_i \beta$. The next step is to make a new linearization from the updated design point and calculate β again. The relative difference between the last two βs is found and FORM converges if this difference is below a certain convergence criterion. See Schneider [38] for further details on how to develop FORM. The last design point is then transformed to real space by

$$x_i^* = \mu_i - \alpha_i \beta \sigma_i \tag{2.28}$$

In a RSM-FORM analysis, FORM iterations are performed for every RSM iteration. The β corresponding to the last converged design point from the previous RSM iteration is compared to the one found in the current. If the relative difference between these are below a certain level, the analysis has converged. The β corresponding to **u*** is used. **u*** is the point along the LSF that has the highest probability of occurring.

Figure 2.16 depicts two FORM iterations performed on the third RSM iteration from Figure 2.15. The FORM linearization and the approximated RS are illustrated in Figure 2.16a in standard normal space, and Figure 2.16b show the same in real space. It is clear that the linearization is not linear in real space. Note that the two FORM linearizations appear as one line since they are very close, and that the design points lie so close that they appear as one point on the plot.

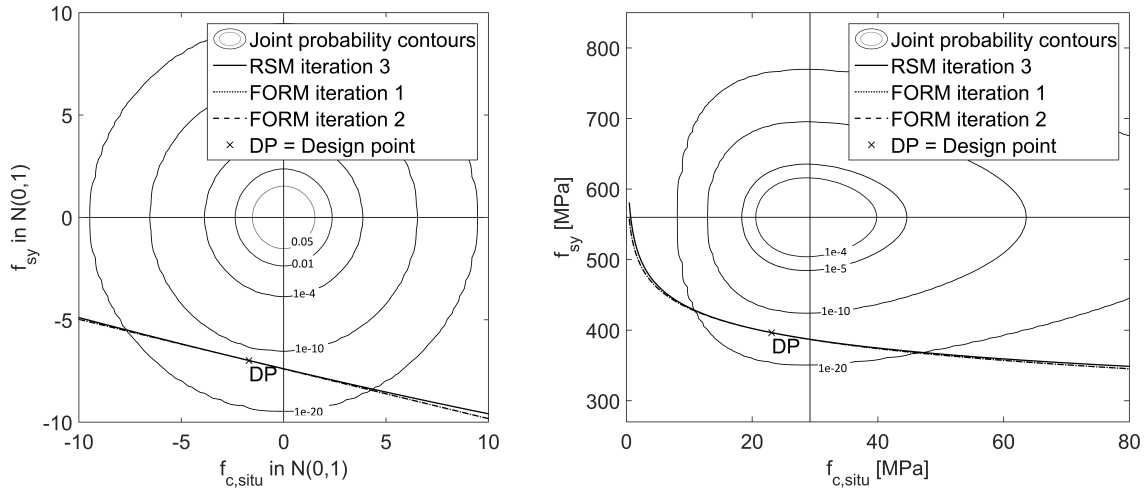

(a) In standard normal space

(b) In real space

Figure 2.16: Two iterations of FORM in standard normal space, with the last RS and joint probability plot

As illustrated for a 2D case in Figure 2.17, the actual LSFs for different systems can take various forms, e.g. linear, curved, irregular and piecewise linear.

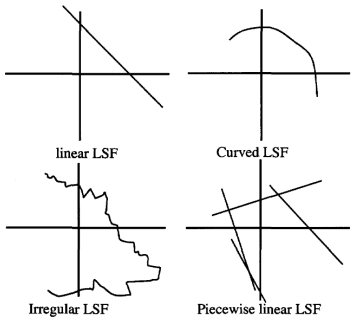

Figure 2.17: Illustrating different shapes of LSFs in 2D [43]

FORM performs better when the LSF is smooth and linear, and will be accurate for a linear LSF. If a highly curved LSF is expected, it is adviced to use a SORM, which takes in second order terms in the Taylor series expansion. For the irregular and/or piecewise linear LSF, FORM and SORM are inadequate, and a system analysis is advised, e.g. the Branch-and-Bound method, [43]. See Thoft Christensen and Murotsu [41] for more details.

In this study, RSM-FORM was analyzed with both analytic and NLFEA LSFEs for the 5.0 m beam. On lengths 2.3 m and 1.5 m, only the analytic RSM-FORM was performed.

The second order polynomial as described in (2.25) was used. The f-factor was set to $f = 3.0$, such that the sample points had coordinates $u_i = 0$ and $u_i = \pm 3$ in standard normal space. The convergence criteria were set to $\epsilon_{FORM} = 0.001$ and $\epsilon_{RSM} = 0.01$. In addition, a side study was performed using analytic LSFEs, where the f-factor varied in the range $0.5 \leq f \leq 5.0$. Another side study was performed using the concrete cylinder strength, f_c, as a stochastic variable, rather than $f_{c,situ}$.

Semi-probabilistic safety formats

The global resistance factor format by *fib* Model Code 2010 is a level I reliability assessment method. It performs one NLFEA that inherently accounts for all failure modes and possible load redistributions. The design resistance is calculated as

$$R_d = \frac{R(f_m, ...)}{\gamma_R \gamma_{RD}} \tag{2.29}$$

where R is the resistance from NLFEA, where mean material properties, f_m, serve as input. γ_R is a global resistance factor and γ_{RD} is a factor accounting for modelling uncertainties. These take the values 1.2 and 1.06, respectively, such that the global safety factor $\gamma_G = \gamma_R \gamma_{RD}$ becomes 1.27. The mean material properties for steel and concrete are defined from their characteristic values in the following manner:

$$f_{ym} = 1.1 f_{yk} \tag{2.30}$$

$$f_{cf} = 1.1 \alpha_{cf} \frac{\gamma_s}{\gamma_c} f_{cfk} \tag{2.31}$$

where f_{ym} is the mean yield stress of the reinforcement steel and f_{yk} is the corresponding characteristic value. f_{cf} is the concrete strength parameter under consideration, and f_{cfk} is its characteristic value. In (2.31), α_{cf} is a coefficient that accounts for long term effects and unfavorable load effects, and γ_s and γ_c are safety factors regarding steel and concrete strengths. Note from the expressions above, the material parameter for steel is increased while concrete is reduced. The reason being that concrete is encumbered with higher uncertainties and is therefore reduced in order to use a common global safety factor [11, 10]. For further details on the global factor method the reader is referred to *fib* Model Code 2010.

The partial safety factor format is another level I reliability assessment method, and accounts for uncertainties by means of design values. The nature of the design values inherently consider the reliability level through material safety factors, γ_i.

$$f_{d,i} = \frac{f_{k,i}}{\gamma_i \gamma_{RD,i}} \tag{2.32}$$

where $f_{k,i}$ is a characteristic value, γ_i is a partial factor for material uncertainties and $\gamma_{RD,i}$ is a factor governing modelling uncertainties and geometric uncertainties for each material. When material, geometric and modelling uncertainties are accounted for, the total partial factors can commonly be taken as $\gamma_C = 1.50$ and $\gamma_S = 1.15$ for calculation of design concrete cylinder strength and steel strength respectively. Here, the PSFs used to assess the different aspects of uncertainty are summarized in Table 2.6.

Table 2.6: PSFs to assess uncertainty by *fib* Model Code 2010 [10]

Material	**Concrete**	**Steel**
Modelling uncertainty	1.05	1.025
Geometric uncertainty	1.05	1.05
Material uncertainty	1.39	1.08
PSF	1.50	1.15

The PSFs assessing modelling, geometric and material uncertainties are multiplied to calculate the partial safety factor for each material. The design resistance is then calculated by

$$R_d = R(f_d) \tag{2.33}$$

Where f_d represents all the design input material parameters in the NLFEA. For a more detailed description of the partial factor method the reader should consult with *fib* Model Code 2010.

The safety formats were tested to check if they gave βs in the range 3-4. This was done by using the stochastic parameters from NLFEA LHS-fit to calculate reliability levels for R_d by $P(R < R_d)$. R is the resistance from LHS-fit. A similar method of checking the reliability levels of safety formats is presented by Schlune et al. [36].

The method of estimation of a coefficient of variation (ECOV) is a third safety format suggested by *fib* Model Code 2010. Here, the global safety factor is assessed using the propagated material uncertainties. The design resistance, R_d, can be expressed in terms of the mean resistance, R_m, which is the capacity from NLFEA using median material parameters, and by a global safety factor for resistance, γ_R:

$$R_d = \frac{R_m}{\gamma_R} \tag{2.34}$$

For a log-normal resistance distribution, *fib* Model Code 2010 states that the safety factor can be represented as

$$\gamma_R = e^{\beta_R V_R} \tag{2.35}$$

where β_R is the target level of reliability of the resistance. V_R is the coefficient of variation of the resistance and can be expressed by

$$V_R = \sqrt{V_f^2 + V_g^2 + V_m^2} \tag{2.36}$$

where V_f denotes material variation, V_g is the geometric variation, and V_m represents the variation in modelling uncertainties. A simplified method to estimate the material uncertainty propagated in the resistance of a structure was proposed by Cervenka [11], and can be expressed as

$$V_f = \frac{1}{1.65} ln \frac{R_m}{R_k} \tag{2.37}$$

where R_k denotes the resistance from NLFEA using characteristic input values.

In this study, this third safety format was used to estimate an upper bound for the modelling uncertainty. The design resistance was taken as the Eurocode 2 design capacity, and the median and characteristic resistance was calculated with NLFEA using median and characteristic material parameters. The target reliability level and variation of geometric uncertainties were taken by Eurocode 0 and Eurocode 2, and the propagated variation in material uncertainties was estimated by (2.37). The upper bound for the modelling uncertainty was then back-calculated by the equations above.

2.4 Uncertainties

There are several ways and opinions on how to sort and divide the uncertainties in a structure. Here, they are divided into three contributions: geometric, material and modelling uncertainties.

Geometric uncertainties regard the physical structure, i.e., deviations in geometric dimensions from the planned structure to the constructed one. Some structures are more sensitive to variations in dimensions, like columns and thin slabs. For structures that are insensitive to geometric imperfections, a coefficient of variation $V_g = 5\%$ can be assumed appropriate [36].

Material uncertainties concern variations in material properties and are commonly described by PDF. The variation of each material is often divided into the variation between suppliers, the variation within a factory and the variation within a produced batch. According to Engen et al. [15], the coefficient of variation in the cylinder strength of concrete may range from $5 - 15\%$, and is dependent on the cylinder strength. Eurocode 2 assumes a coefficient of variation of 15% for concrete. Both sources report a typical coefficient of variation for steel to 5%.

Modelling uncertainties contain all uncertainties not covered by the two aforementioned. This regards all uncertainties accumulated from a structure in real life to the one that is used for calculations. This includes the selection of a static model, to a finite element model, to the choice of input parameters like material model and solution method, and the interpretation of the results. For a problem with many possible input variables, these must be reduced to a feasible amount while still retaining the model's ability to describe the response accurately [14]. It is important to note the difference between errors in the analysis procedure and errors concerning the idealization of physical response. Both aspects are complementary to the total accuracy, as a robust analysis procedure without a proper description of the material behavior will not enhance the model [15]. Also included is the uncertainty regarding the probabilistic model, and method of reliability assessment [44].

It is difficult to quantify the modelling uncertainty on a general basis, since one model can perform differently when applied to different scenarios. One method of quantifying the modelling uncertainties is proposed by *fib* Model Code 2010 by a model variable $m = \frac{R_{Exp}}{R_{NLFEA}}$ which takes the response from experiments, R_{Exp}, and response from NLFEA, R_{NLFEA}. This requires that the response from experiments are known. As mentioned, the coefficient of variation is not a constant that can be widely applied for all models. Engen et al. [15] performed 38 benchmark analyses, and suggested a log-normally distributed modelling uncertainty with a mean $\mu_m = 1.10$ with a coefficient of variation of $V_m = 12\%$. On the other hand, Schlune et al. [36] found that the modelling uncertainty for under reinforced beams failing in bending had coefficients of variation from $5 - 15\%$, whereas for shear failure this varied from $10 - 40\%$. Schneider [38] states that the analytic calculation model of a reinforced concrete beam in bending is good, so the value of the modelling coefficient is often just a few percent. Therefore for beams failing in bending, the mean of m is often close to one, $\mu_m \approx 1$.

In other words, the modelling uncertainties vary greatly, and it is often the engineer's judgment to determine the modelling uncertainty, resulting in subjective results. Therefore, when using NLFEA, the model should be validated for the problem at hand through benchmark experiments.

2.5 Method for limit state function evaluations

In this section, the method for both NLFEA and analytic LSFEs are summarized.

2.5.1 Non-linear finite element analysis

The method for NLFEA LSFEs is a product of the optimization study shown in Appendix A. The method for NLFEA LSFEs consists of the solution strategy and post-processing, as illustrated in Figure 2.18.

Figure 2.18: Method for NLFEA LSFEs

Diana was the chosen software for NLFEA in this study. The beam was modeled with a reference load $P1 = 100$ kN. The mesh for the 5.0 m beam is shown in Figure 2.19.

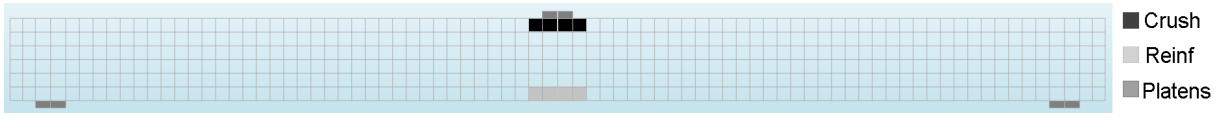

Figure 2.19: FE model of the 5.0 m beam

The black elements in Figure 2.19 denoted *Crush* show where concrete strains were extracted, and the light gray elements *Reinf* show where reinforcement strains were extracted for post-processing. Platens, illustrated by dark gray elements, were used under the point load and over the supports to avoid singularities. The load and support were applied as point restraints to these platens, and details are are illustrated in Figure 2.20. Interface elements were needed to get the wanted interaction between the concrete and platen elements.

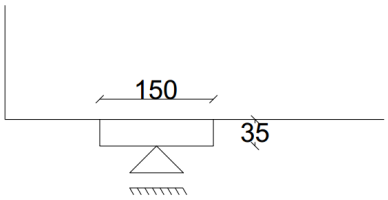

Figure 2.20: Platen details, lengths in mm

For the purpose of the reliability analyses in this study, about a thousand NLFEA were performed, using a variety of concrete and steel strengths. To make this feasible, the solution strategy was coded in a Python-script, where the only input values were the two stochastic variables. To monitor failure, the principal strains in the integration points for the element group named *Crush*, and the reinforcement stresses in the integration points

for the element group called *Reinf* were printed to an output file. The displacement of the bottom node in the mid-span, the reaction forces and the number of iterations in each increment step were also printed. The output file was post-processed with a Matlab script.

In the following, the method for NLFEA LSFEs is summarized in tables. Options for the model that are not specified here, were taken as default values in Diana defaults. The NLFEA analysis procedure is presented in Table 2.7. Table 2.8 shows the options used for the meshing of the 5.0 m beam. Failure was defined in the post-processing with the fixed strain failure definition defined in Table 2.9. Table 2.10 and 2.11 summarizes the reinforcement and concrete models, respectively. The material models for the platens and interface elements are already presented in Table 2.4 and 2.5, respectively.

Table 2.7: NLFEA analysis procedure

Property	**Value**
User defined load steps	0.1(100)
Arc-length method	Updated Normal Plane
Control type	Regular (no control set)
Unloading determination	Sign change
Iterative solver	Regular N-R
Max iterations	100
Line search:	
Lower bound	0.1
Upper bound	1
Maximum number of searches	5
Energy criterion [Psi]	0.8
Regula Falsi interval Delta eta	0.1
Convergence norm (either):	
Energy	< 0.001
Force	< 0.01
No convergence	Continue
Abort criterion	10 000 for both
Solution method	Sparse-Cholesky with convergence criterion 10^{-8}

Table 2.8: FE model

Property	**Value**
Element	Q8 with 2x2 Gauss integration
Element size	66.7 mm (75.0 mm)
Interface element	CL12I with 3-point Newton-Cotes integration
Reinforcement	Modelled as embedded

Table 2.9: Fixed strain failure definition (excerpt from Table A.3)

Failure definition	**Failure**
Fixed strain failure	The strain in the integration points in *Crush* limits the region where the max converged load is searched for. The strain limit was set to 1.8‰, which is ϵ_{c1} for the weakest concrete in Eurocode 2.

Table 2.10: Material model for the reinforcement

Property	**Value**
Constant:	
Material model	Isotropic bi-linear elasto-plastic
Young's modulus	$E_s = 200\,000$ MPa
Ultimate strain	$\epsilon_{su} = 7.5$ %
Poisson's ratio	$\nu_s = 0.0$
Variable:	
Yield strain	$\epsilon_{sy} = \frac{f_{sy}}{E_s}$
Ultimate stress	$f_{su} = 1.25\ f_{sy}$
E_{har}	$\frac{f_{su} - f_{sy}}{\epsilon_{su} - \epsilon_{sy}}$

Table 2.11: Material model for the concrete

Property	**Value**
Constant:	
Crack model	Total strain-based rotating crack
Crack bandwidth	Automatic
Tensile behavior	Exponential stress-strain relationship
Residual tensile strength	0 MPa
Compressive behavior	Parabolic stress-strain relationship
Residual compressive strength	0 MPa
Reduction due to lateral cracking	Vecchio & Collins 1993
Min. reduction factor due to lateral cracking	$\beta_{\sigma}^{min} = 0.6$
Poisson's ratio reduction	Damage based
Stress confinement effect	Selby and Vecchio
Initial Poisson's ratio	$\nu_c = 0.15$
Variable:	
Tensile strength	$f_{ct,situ} = 0.3(f_{c,situ} - 6)^{2/3}$
Fracture energy	$G_{F,situ} = 73 f_{c,situ}^{0.18}$
Compressive fracture energy	$G_{C,situ} = 250 G_{F,situ}$
Young's modulus	$E_{c,situ} = E_{c0} \left(\frac{f_{c,situ}}{10}\right)^{1/3}$

2.5.2 Analytic

The beam was assumed to have two possible failure modes depending on its length, namely moment and shear. Eurocode 2 capacity equations were modified to give median values, meaning each observation has a 50 % change of being higher than this. Modified capacity equations are derived and presented in Appendix B, as well as summarized in this section. Beam load capacity is the minimum of

$$R = \min[P_M = \frac{M_r}{4L}, P_V = 2V_r] \tag{2.38}$$

where moment capacity, M_r, is expressed by (2.40) to (2.44), assuming concrete crushing and steel strain above yield. Shear flexure capacity, V_r, is expressed by (2.39). L is the

beam length. The capacity input variables were $f_{c,situ}$ and f_{sy} as presented in 2.1.2. In addition, the concrete ultimate strain was set to $\epsilon_{cu} = 3.5‰$ and the tensile strength was set to zero as recommended by Eurocode 2. For steel, the same bi-linear material model as described in Table 2.10 was used. Note that (2.43) should be solved using iterative methods, ranging ϵ_s from zero to ϵ_{su}.

$$V_r = 0.20k(100\rho_l f_{c,situ})^{1/3} b_w d \tag{2.39}$$

$$M_r = F_c(0.2 + \frac{1}{2}0.8)\alpha d + F_t(1-\alpha)d \tag{2.40}$$

$$F_c = \eta\lambda\omega b d f_{c,situ} \qquad \text{and} \qquad F_t = E_{s,mod}\epsilon_s A_s \tag{2.41}$$

$$\omega = \frac{\epsilon_{cu}}{\epsilon_s + \epsilon_{cu}} \tag{2.42}$$

$$(E_{s,mod}\rho)\epsilon_s^2 + (E_{s,mod}\rho\epsilon_{cu})\epsilon_s - \eta\lambda\epsilon_{cu} f_{c,situ} = 0 \tag{2.43}$$

$$E_{s,mod} = \frac{f_{sy} + E_{har}(\epsilon_s - \epsilon_{sy})}{\epsilon_s} \tag{2.44}$$

Figure 2.21 show how the moment and shear parts of the analytic LSF by (2.38) looks for the 2.3 m beam with a load of 105 kN. The failure domain is illustrated in gray.

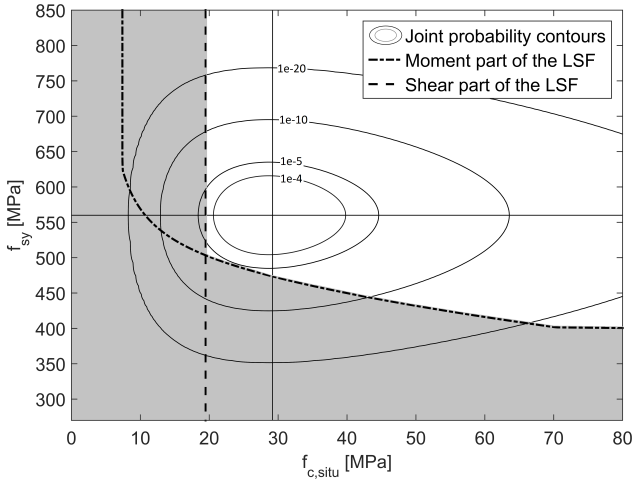

Figure 2.21: Example of LSF

Chapter 3

Results

In order to assess reliability using NLFEA, a general method for NLFEA LSFEs was needed, and was hard to accomplish. Therefore, only the 5.0 m beam was analyzed with NFLEA. This chapter presents a brief summary of the results of the optimization study on the method for NLFEA LSFEs presented in Appendix A. Then, the results from reliability analyses are presented. The analytic Monte Carlo analyses were regarded as benchmarks to compare the other reliability analyses to. LHS-fit and RSM-FORM were performed using both NLFEA and analytic LSFE, while LHS-count was only used with analytic LSFs. The safety formats were assessed using NLFEA with specific material parameters. Analytic LSFEs were applied to all beam lengths.

3.1 Optimization of the method for NLFEA LSFEs

As stated in Section 2.3.2, RSM-FORM performs better for a relatively smooth LSF. In order to achieve this using NLFEA for LSFEs, optimization was needed. In this section, an overview of this process for the 5.0 m beam is presented, as well as a briefing on the 1.5 m beam. A more thorough description is found in Appendix A.

Figure 3.1 illustrates two load capacity surface plots, one using manual load control and one using the UNP method. The methods are summarized in Tables A.1 and A.2. Both plots have the analytic evaluation overlayed with see-through green color. As seen in Figure 3.1a, the manual load control provides an erratic load capacity surface. For higher

material strengths, higher capacities are expected, however this is not always the case. In Figure 3.1b, a surface plotted with results using the UNP method is shown. This is very smooth compared to the manual load control, although some inconsistencies can be seen relative to the analytic evaluations. Both methods used the fixed strain failure definition. Other failure definitions were tested, and are presented in Appendix A.

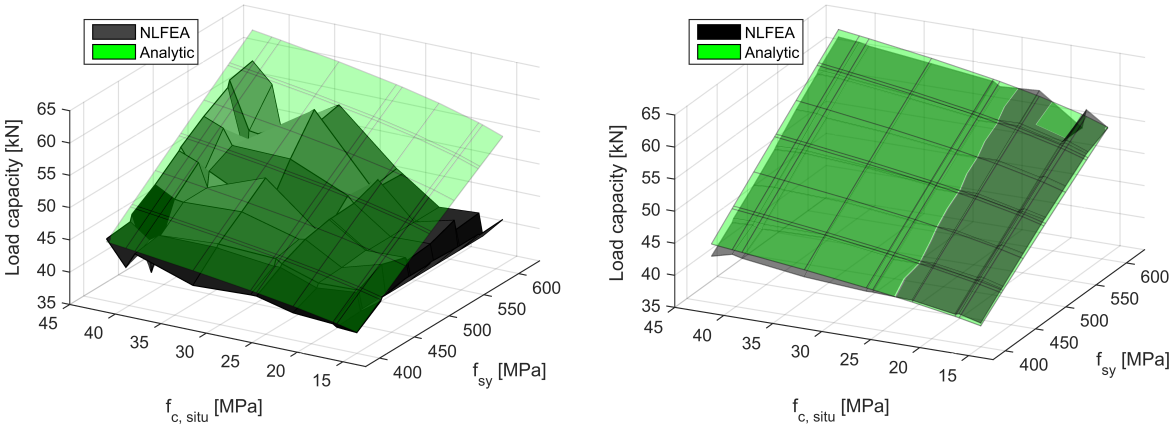

(a) Manual load control

(b) The UNP method

Figure 3.1: Load capacity surface plots using the fixed strain failure definition

To better illustrate the inconsistencies for the UNP method, results are also plotted in Figure 3.2 for specified steel and concrete strengths.

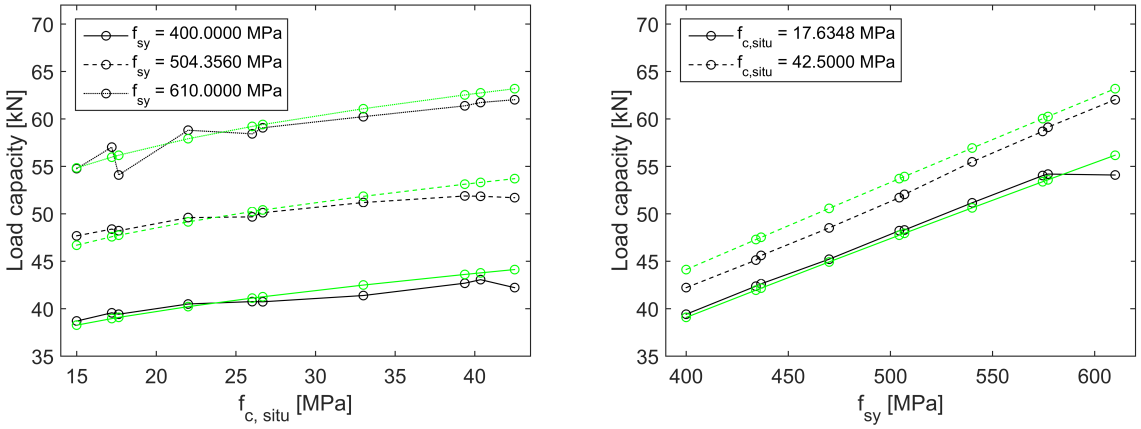

(a) Load capacities depending on $f_{c,situ}$

(b) Load capacities depending on f_{sy}

Figure 3.2: Load capacity plots extracted from the surface plot in Figure 3.1b. NLFEA load capacity in black, and analytic in green

Although the UNP method worked for the 5.0 m beam, this method was not applicable when changing the beam length to 1.5 m. It resulted in highly inconsistent capacities. Some efforts were done to remedy this by applying different failure definitions in the post-processing. No general method was obtained for NLFEA LSFEs that was consistent and accurate for a variation of material inputs.

3.2 Reliability methods

In this section, results from the reliability studies are presented. Firstly, a compilation of βs are shown before results from each method is presented in greater detail. For each beam length, the load corresponding to $\beta_R = 3.04$ by the capacity equation in Eurocode 2 was applied. This corresponds to 40 kN for 5.0 m beam, and 73 kN for the 1.5 m and 2.3 m beam. In addition, other loads were also applied, such that the reliability indexes calculated in this study were in the range $7.2 < \beta < -4.0$.

The reliability analyses performed on the 5.0 m beam were: Analytic Monte Carlo, analytic RSM-FORM, NLFEA RSM-FORM, analytic LHS-fit, analytic LHS-count and NLFEA LHS-fit with $N = 50$. Table 3.1 summarizes the βs found with each method, as well as their respective relative error to Monte Carlo. Due to the large number of analyses required for high βs, the Monte Carlo method was not applied for a load of 40 kN. Note the greater errors for NLFEA when subjected to higher loads.

Table 3.1: Compilation of βs for Monte Carlo, RSM and LHS-fit simulations for analytic and NLFEA LSFEs on the 5.0 m beam

LSFE type	**Load [kN]**	**40**	**45**	**50**	**55**	**60**
Analytic	Monte Carlo β	-	4.903	2.620	0.3686	-1.816
Analytic	RSM-FORM β	7.232	4.913	2.621	0.3692	-1.832
	β-Error [%]	-	0.20	0.02	0.16	-0.90
NLFEA	RSM-FORM β	7.196	4.917	2.616	0.2197	-2.055
	β-Error [%]	-	0.28	-0.15	-40.4	-13.1
Analytic	LHS-fit β	7.031	4.810	2.588	0.3664	-1.855
	β-Error [%]	-	-5.53	-4.93	-4.86	-1.43
NLFEA	LHS-fit β	7.118	4.801	2.484	0.1676	-2.149
	β-Error [%]	-	-2.08	-5.19	-54.5	-18.4

To further illustrate the βs for the 5.0 m beam, these are plotted against the load capacity in Figure 3.3. The reliability methods included here are the Monte Carlo analytic as a benchmark, as well as NLFEA RSM-FORM and NLFEA LHS-fit.

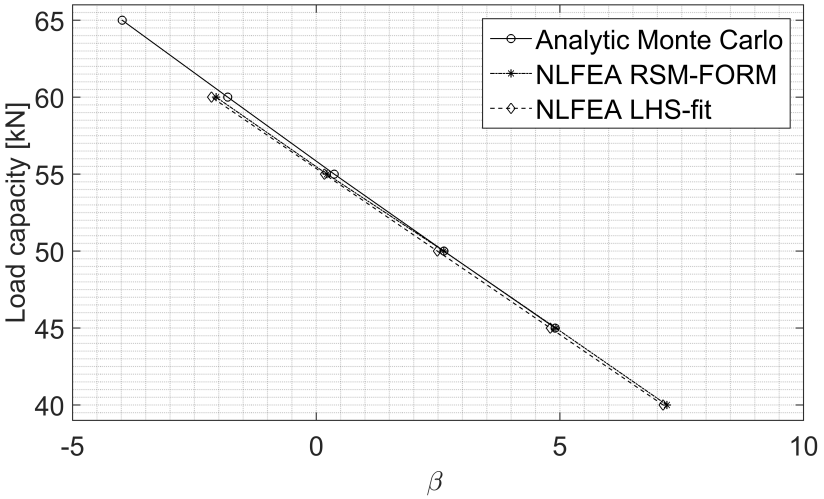

Figure 3.3: Load capacity vs β for the 5.0 m beam

In Table 3.2, βs are tabulated for analytic LSFEs. LHS-fit and LHS-count results were taken as the mean of 10 runs, each with $N = 10^6$. βs are given for the three lengths, each subjected to three loads so that the range of β is corresponding to engineering practices. Note that RSM-FORM seem to overestimate β, while LHS-fit seems to underestimate β.

Further, RSM-FORM errors are consistently below 0.5% for the 1.5 m and 5.0 m beam, but for the 2.3 m beam the errors are larger at loads 100 kN and 105 kN for RSM-FORM. LHS-fit results are most inaccurate for the 1.5 m beam.

Table 3.2: β using analytic LSF with Monte Carlo, RSM-FORM, LHS-fit and LHS-count

L [m]		**1.5**			**2.3**			**5.0**	
Load [kN]	**95**	**100**	**105**	**95**	**100**	**105**	**45**	**50**	**55**
Monte Carlo β	5.117	3.992	2.932	5.100	3.966	2.873	4.903	2.620	0.3686
RSM-FORM β	5.108	3.993	2.932	5.108	3.993	2.958	4.913	2.621	0.3692
β-error [%]	-0.19	0.02	0.01	0.15	0.66	2.94	0.20	0.02	0.16
LHS-count β	5.095	3.993	2.932	5.113	3.964	2.877	4.891	2.617	0.3674
β-error [%]	-0.44	0.02	0.01	0.26	-0.06	0.13	-0.25	-0.15	-0.33
LHS-fit β	4.568	3.665	2.762	4.950	3.901	2.853	4.806	2.589	0.3719
β-error [%]	-10.7	-8.19	-5.80	-2.93	-1.64	-0.71	-1.97	-1.22	0.90

3.2.1 RSM-FORM

As mentioned, both analytic and NFLEA LSFEs were used with RSM-FORM for the 5.0 m beam. The location of their design points are shown in Figure 3.4 on the joint probability contour plot.

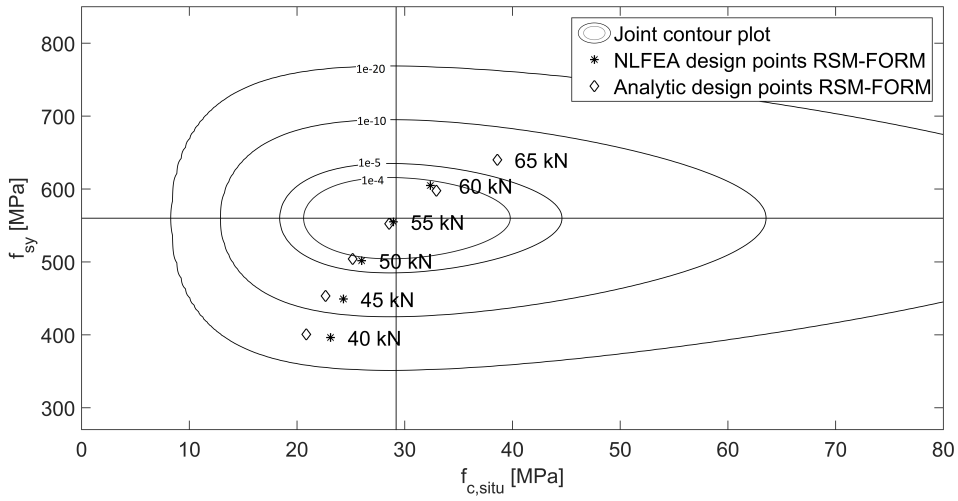

Figure 3.4: Analytic and NLFEA design points for several loads on the 5.0 m beam

Figure 3.5a and 3.5b illustrate the analytic LSF, RSM approximations and design points for analytic and NLFEA RSM-FORM, for a load of 40 kN and 60 kN, respectively. Note the difference in accuracy of the RSM approximation and the distance from design points to origo for the two different loads.

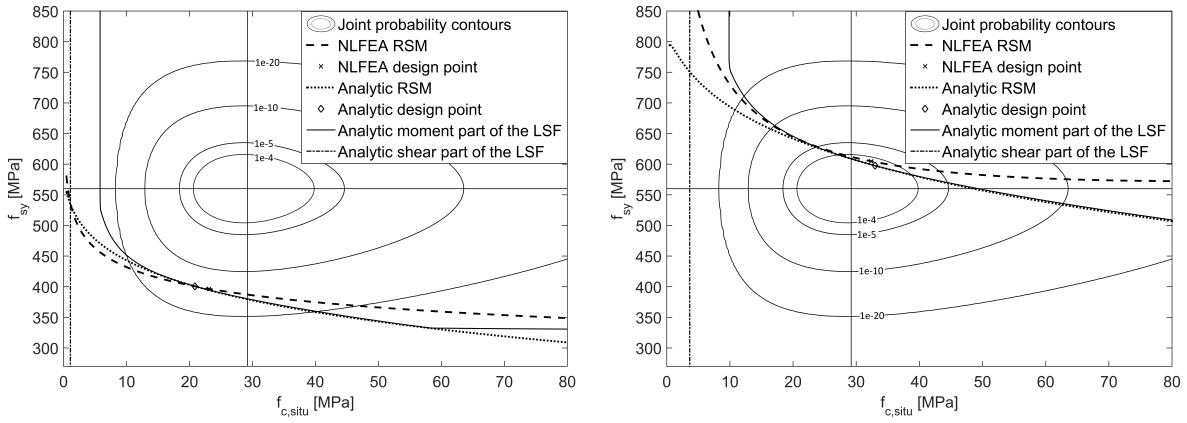

(a) For P = 40 kN

(b) For P = 60 kN

Figure 3.5: RSM approximation and design points for NLFEA and analytic RSM-FORM on 5.0 m beam. Also plotted is the analytic LSFs

Table 3.3 gives the reliability results obtained with NLFEA RSM-FORM. It is important to note that for 55 kN, the ϵ_{RSM} is changed from 1% to 5% due to β being very close to zero, resulting in large relative error between iterations.

Table 3.3: NLFEA RSM-FORM results for the 5.0 m beam

Load [kN]	$\boldsymbol{\beta}$	$\boldsymbol{\alpha_c}$	$\boldsymbol{\alpha_s}$	**Design point [MPa]**	**# RSM iterations**
40	7.196	0.2354	0.9719	23.1, 396	3
45	4.917	0.2701	0.9628	24.3, 449	4
50	2.616	0.2713	0.9625	26.0, 502	8
55	0.2197	0.2765	0.9610	29.0, 555	2
60	-2.055	0.3646	0.9312	32.4, 605	2

One NLFEA RSM-FORM was also performed with concrete cylinder strength, hereon referred to as concrete non-in-situ strength, and a load of 40 kN. The analysis started in the median values, as was done using $f_{c,situ}$. Here, FORM ran 745 000 iterations in the second RSM iteration without convergence, and was manually stopped. Then, a new

RSM-FORM analysis was performed, this time starting in $P_0 = [25, 390]$ MPa. This location was chosen based on results obtained using $f_{c,situ}$. Figure 3.6 shows the location of the design point in reference to the response surface and its FORM linearizations over the joint PDF. Note that the RS approximation in Figure 3.6b curves the other way.

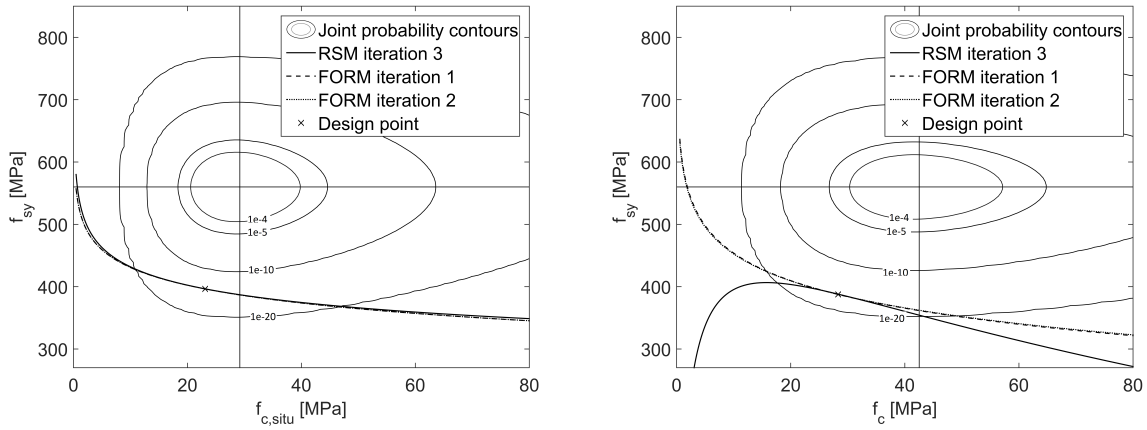

(a) Using in-situ values for concrete

(b) Using non-in-situ values for concrete

Figure 3.6: Plots showing the design point, contour of joint PDF, the last response surface and its linearizations

Table 3.4 shows the reliability results from the non-in-situ RSM-FORM analysis. Note that β is higher using non-in-situ concrete, and that only two RSM iterations were needed.

Table 3.4: NLFEA RSM-FORM results for the 5.0 m beam using non-in-situ concrete

Load [kN]	$\boldsymbol{\beta}$	$\boldsymbol{\alpha_c}$	$\boldsymbol{\alpha_s}$	**Design point [MPa]**	**# RSM iterations**
40	7.894	0.3585	0.9335	28.5, 387	2

Figure 3.7 illustrates the analytic load capacity surface of the 2.3 m beam. The surface consists of three smooth surfaces, separated by two white ridges. The surface located to the right represents the shear load capacity and the possibility of a shear failure mode. The two surfaces to the left represent different types of moment load capacities and the possibility of a moment failure mode. The smallest of these two, located furthest left, represents moment failure mode where the steel reaches its ultimate strain, and the larger in the middle represents moment failure due to failure of the compressive zone. It's notable that using Eurocode 2 design capacities, the transition zone would be at 2.7 m instead of 2.3 m.

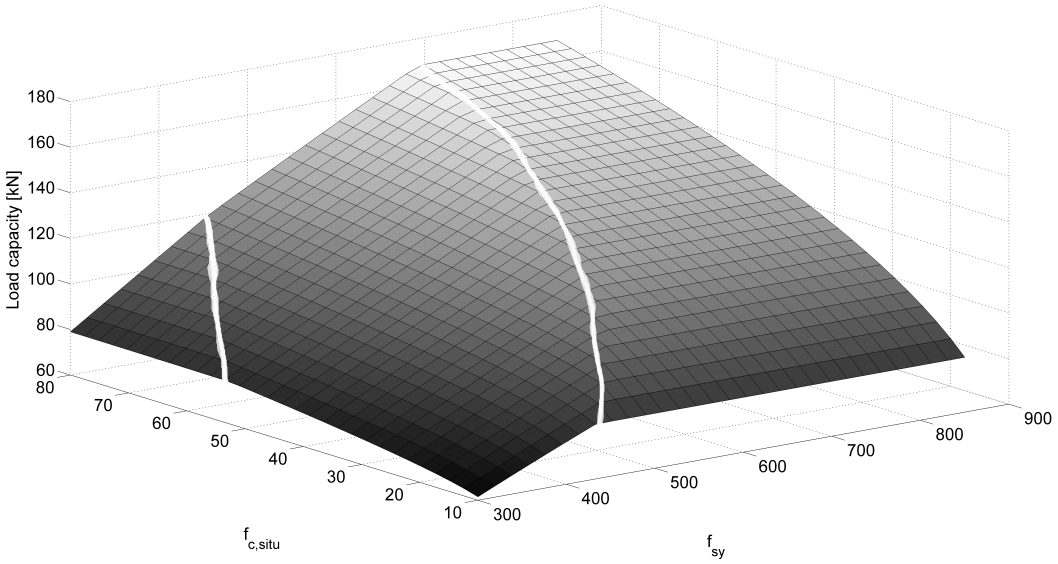

Figure 3.7: Analytic load capacity surface for the 2.3 m beam with varying material strengths

A selection of reliability results for the 5.0 m beam is given in Table 3.5 for analytic RSM-FORM. This gives comparable βs to NLFEA RSM-FORM, but a notable difference in α-values.

Table 3.5: Analytic RSM-FORM results for the 5.0 m beam

Load [kN]	β	$\boldsymbol{\alpha_c}$	$\boldsymbol{\alpha_s}$	**Design point [MPa]**	**# RSM iterations**
40	7.233	0.3405	0.9403	20.8, 401	3
45	4.913	0.3791	0.9254	22.6, 454	3
50	2.621	0.4153	0.9097	25.1, 504	3
55	0.3692	0.4491	0.8935	28.5, 552	2
60	-1.832	0.4817	0.8764	33.0, 560	2

A selection of reliability results for the 2.3 m beam with different loads are given in Table 3.6. It is notable that α-values change drastically depending on the load.

Table 3.6: Analytic RSM-FORM results for the 2.3 m beam

Load [kN]	β	α_c	α_s	**Design point [MPa]**	**# RSM iterations**
73	10.23	0.2887	0.9574	19.4, 331	4
95	5.108	1.0000	0.0000	14.4, 560	7
100	3.993	1.0000	0.0000	16.8, 560	4
105	2.958	0.9892	0.1464	19.5, 550	5

A variational study was performed on the 2.3 m beam, varying the f-factor. The effect of this on the RSM-FORM is shown in Figure 3.8, where the f-factor takes the values 1.0 and 3.0, respectively. For an f-factor of 1.0, all sample points were within the shear LSF, while using an f-factor of 3.0 caused one sampling point to be affected by the moment LSF, which results in the different RSs.

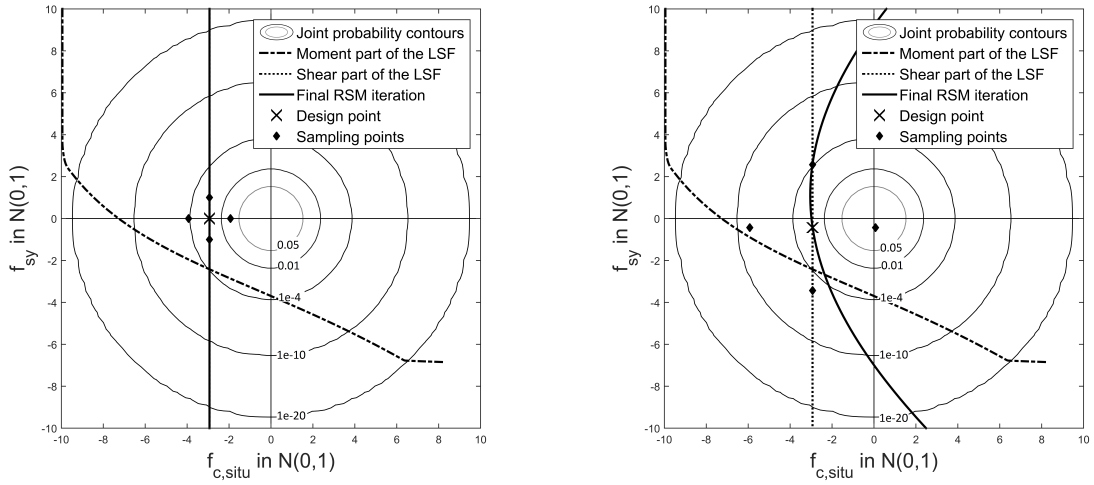

(a) Using an f-factor of 1.0

(b) Using an f-factor of 3.0

Figure 3.8: Showing the analytic moment and shear LSF, the analytic RS and its design point for two f-factors

The effect of varying the f-factors is further illustrated in Figure 3.9. The two loads with high errors from Table 3.2, 100 kN and 105 kN, were analyzed with varying the f-factors from 0.5 to 5.0. The RSM-FORM βs from Table 3.2 are found at $f = 3.0$. Monte Carlo βs are presented as dashed lines for each of their RSM-FORM counterpart, and are constant for all f-factors. The figure illustrates systematic error discrepancy from Monte Carlo β for the 100 and 105 kN loads, f-factor dependencies at higher f-factors, and sporadic

erroneous convergence for 100 kN load at f-factors of 0.5 and 2.2.

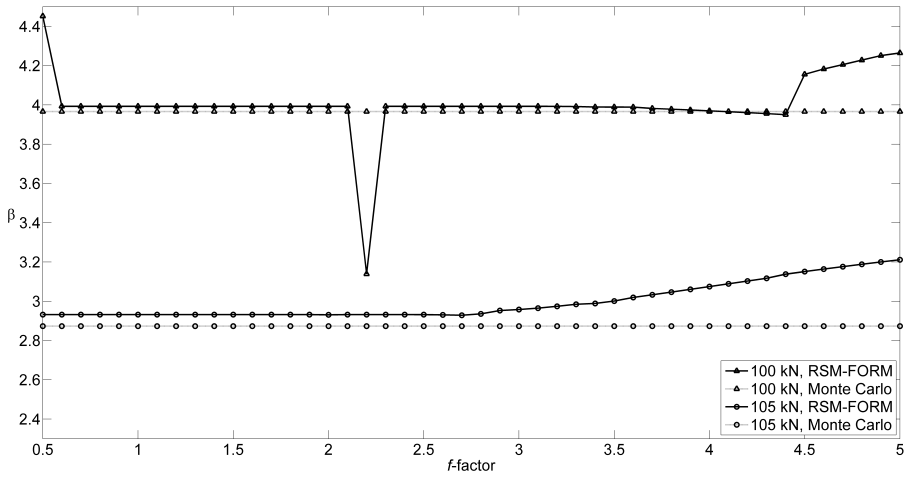

Figure 3.9: f-factor dependency of RSM-FORM β-results for the 2.3 m beam subjected to loads 100 and 105 kN. Monte Carlo β for comparison

A selection of reliability results for the 1.5 m beam with different loads are given in Table 3.7. Note that only concrete influence the results.

Table 3.7: Analytic RSM-FORM results for the 1.5 m beam

Load [kN]	$\boldsymbol{\beta}$	$\boldsymbol{\alpha_c}$	$\boldsymbol{\alpha_s}$	**Design point [MPa]**	**# RSM iterations**
73	10.83	1.0000	0.0000	6.5, 560	3
95	5.108	1.0000	0.0000	14.4, 560	2
100	3.993	1.0000	0.0000	16.8, 560	2
105	2.932	1.0000	0.0000	19.5, 560	2

3.2.2 Latin hypercube sampling

Figure 3.10 shows load capacities for the 5.0 m beam obtained with NLFEA as histograms with $N = 50$ samples. The load capacities were approximated with normal PDFs from which βs were obtained. The fitting shows that normal PDF is just an approximation.

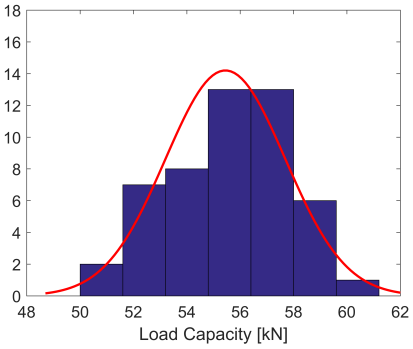

(a) Sample set 1

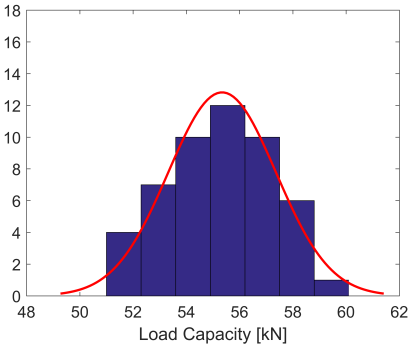

(b) Sample set 2

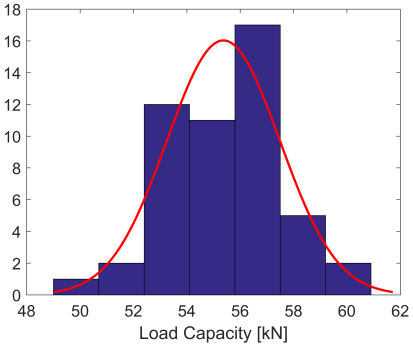

(c) Sample set 3

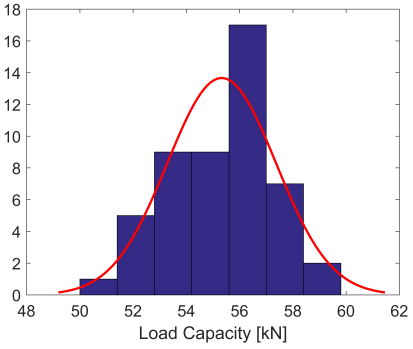

(d) Sample set 4

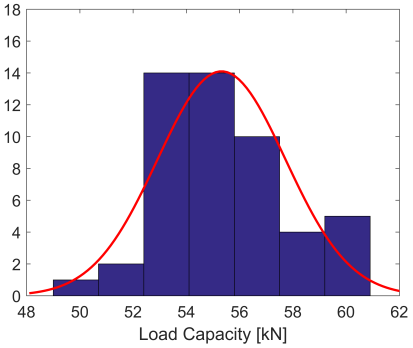

(e) Sample set 5

Figure 3.10: Histograms fitted with normal PDF for $N = 50$

Table 3.8 shows βs averaged over five sample sets together with their standard deviations for NLFEA and analytic LSFEs. Statistical parameters for the NLFEA load capacities were $\mu = 55362$ N and $\sigma = 2167$ N. Note that σ_β decreases towards the mean value of the load capacity.

Table 3.8: β using Monte Carlo, and analytic and NLFEA LHS-fit using 5 sample sets of $N = 50$ for the 5.0 m beam

LSFE method	**Load [kN]**	**40**	**45**	**50**	**55**	**60**
Analytic	Monte Carlo β	-	4.903	2.620	0.3686	-1.816
Analytic	LHS-fit β	7.031	4.810	2.588	0.3664	-1.855
	σ_β	0.590	0.402	0.213	0.024	0.165
	β-Error [%]	-	5.53	4.93	4.86	1.43
NLFEA	LHS-fit β	7.117	4.801	2.484	0.1676	-2.149
	σ_β	0.449	0.302	0.155	0.021	0.142
	β-Error [%]	-	2.08	5.19	54.5	18.4

Table 3.9 shows βs obtained from curve fitting and by counting failure outputs from analytic LSFEs. These were calculated for three lengths and three sample sizes. Every β has a corresponding standard deviation and these were found by performing the analyses 1000, 100 and 10 times for $N = 50$, $N = 10^3$ and $N = 10^6$, respectively.

Table 3.9: βs with standard deviations from LHS-fit and LHS-count

Length [m]		**1.5**		**2.3**		**5.0**	
Load [kN]		**105**		**105**		**50**	
LHS type		**fit**	**count**	**fit**	**count**	**fit**	**count**
$N = 50$	β	2.737	-	2.839	-	2.595	-
	σ_β	0.072	-	0.147	-	0.161	-
$N = 10^3$	β	2.761	2.948	2.853	2.900	2.590	2.649
	σ_β	0.004	0.100	0.028	0.112	0.031	0.140
$N = 10^6$	β	2.762	2.932	2.853	2.877	2.589	2.617
	σ_β	$< 10^{-5}$	$< 10^{-3}$	$< 10^{-3}$	0.003	0.001	0.004

Figure 3.11 shows βs in the shear dominant region and in the transition zone. The load capacities were calculated using analytic LSFs, and βs were found from both curve fitting and counting for sample size $N = 10^6$ and subjected load equal to 105 kN.

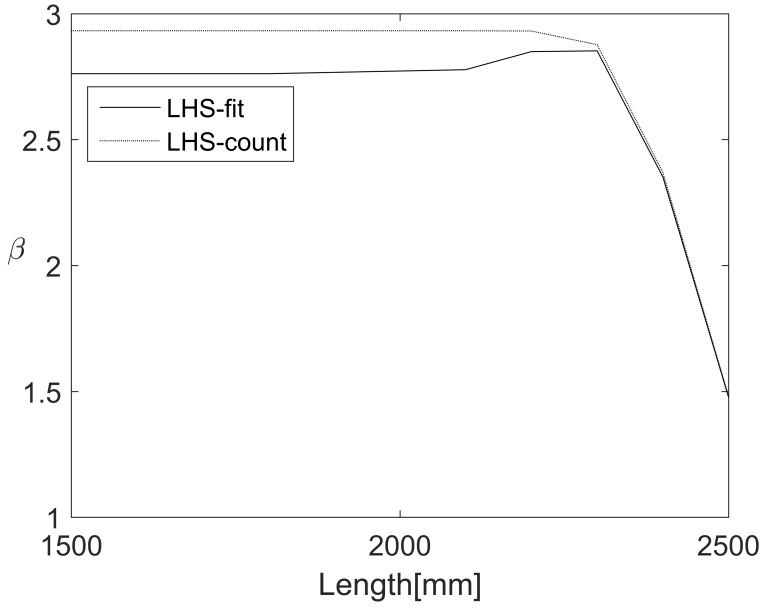

Figure 3.11: βs for different lengths subjected to a load of 105 kN

3.2.3 Safety formats

For both safety formats, input values in the NLFEA were calculated according to Section 2.3.2. βs were obtained for the design resistances of the formats by using the statistical parameters obtained from NLFEA LHS-fit. The results are summarized in Table 3.10.

Table 3.10: Safety format results

Safety format	**Concrete** [MPa]	**Steel** [MPa]	γ_{RD}**(concrete/steel)** [-]	R_d [N]	β [-]
Global factor	$f_{cm} = 25.30$	$f_{ym} = 550.0$	1.06	42 433	5.96
Partial factor	$f_{cd} = 18.18$	$f_{yd} = 402.6$	1.10/1.08	40 330	6.93

3.3 Uncertainties

Since only two stochastic material parameters were used, the reliability results only include some material uncertainties, while geometric and modelling uncertainties were not implemented. Here, attempts to estimate some of these are presented.

3.3.1 Material uncertainties

Several methods are described in the literature to estimate material uncertainties. As stated in Section 2.4, the Eurocode 2 commentary [21] gives a variation of 15% for concrete and a coefficient of variation for steel 5%. Their combined variation will then yield a material uncertainty by the Eurocode [21] of $V_{f,EC} = 15.81\%$. The actual coefficient of variation in the steel and concrete probability distributions are respectively $V_{f,c} = 10.53\%$ and $V_{f,s} = 4.18\%$, which yields a total material uncertainty $V_{f,actual} = 11.32\%$. The ECOV method presented in (2.37) estimates the coefficient of variation of the resistance due to the material to $V_f = 7.83\%$. Since this variation is calculated based on the resistance, it estimates the propagated material uncertainty.

Note that $V_{f,EC}$ and $V_{f,actual}$ are pure material uncertainties that can be used for material PSFs, while the ECOV method for V_f indicates how the material uncertainty affects the global resistance.

3.3.2 Modelling uncertainties

As stated in 2.4, the modelling uncertainties lie in the range of 5-15% for an under reinforced beam failing in bending. An attempt to estimate the upper bound of the modelling uncertainty for the 5.0 m beam failing in bending is done using (2.34) to (2.37). The NLFEA capacity using the mean and characteristic values were $R_m = 55510$ N and $R_k = 48780$ N, respectively. The design resistance was calculated by Eurocode 2 to, $R_d = 39884$ N. From this, a global resistance factor was calculated to $\gamma_R = 1.392$, with a corresponding coefficient of variation for the resistance to $V_R = 10.74\%$. The coefficient of variation for the material was calculated by the ECOV method to $V_f = 7.83\%$, and the coefficient of variation for geometry was set to $V_g = 5\%$ in accordance with *fib* Model Code 2010. Then the estimation of the upper bound of the modeling uncertainty results in $V_m = 5.4\%$.

It is important to understand the underlying assumptions of this method of estimating the modelling uncertainties. First, R_d is the design capacity according to Eurocode 2 for beams failing in bending, and is not necessarily equal to the design resistance using NLFEA. Moreover, the estimated upper limit indicates the allowable modelling uncer-

tainties, while still expecting a design capacity equal to or larger than the Eurocode 2 design capacity. Also, it is assumed that the resistance is log-normally distributed.

Chapter 4

Discussion

To make the reliability methods feasible, only $f_{c,situ}$ and f_{sy} are represented as stochastic variables. All other LSF parameters are considered deterministic or related to either of the two stochastic variables. With this simplification, the geometric and modelling uncertainties are not included in the LSF, and the material uncertainty is also affected. The limited uncertainties included could be one of the reasons for the overall high βs compared to the target β_R from Eurocode 0. This also affects the influence factors for RSM-FORM, especially for NLFEA.

4.1 Method for NLFEA LSFEs

As the load capacity surfaces for the 5.0 m beam in Figure 3.1a and 3.1b show, the method for NLFEA LSFEs heavily affects the shape of the surface. In short, the results in Appendix A primarily indicate four things; (1) for feasibility reasons, the method for NLFEA LSFEs needs to be applicable for a wide variety of material parameters, meaning that manual load control seems unfeasible for reliability studies of concrete, (2) some form of post-processing should be used due to the imperfections of the NLFEA solution strategy, (3) the UNP method with fixed strain failure definition could be used as a method for NLFEA LSFEs when analyzing reinforced concrete failing in bending, although its implementation in this study seems to have limited validity with concern to the range of the stochastic variables, and (4) the method of NLFEA LSFEs gave slightly different results on different computers using the same input.

The error introduced by the method for NLFEA LSFEs to the exact load capacity surface should be minimal and conservative. No experiment was done, and it is therefore not possible to conclude whether the discrepancies were conservative or not. However, since the modified analytic equation for bending capacity is derived from force and moment equilibrium, it can be assumed to model bending failure with high accuracy. The method for NLFEA LSFEs is compared to the analytic bending equation.

With this comparison, manual load control is very conservative, and at the same time the load capacity surface is highly inconsistent. The UNP method with fixed strain failure definition manages to replicate the analytic formulas for bending failure with only small errors, although it calculates a higher load capacity for some material parameters. These small errors indicate that the modelling uncertainty for the NLFEA is within reasonable limits. To get the same capacities as Eurocode 2, the modelling uncertainty using NLFEA needs to be below 5.4%, as calculated in Section 3.3.1. This is in the lower range of the modelling uncertainty suggested by Schlune [36]. With the high resemblance to the analytic formulas, this might be the case. However, the exact modelling uncertainty for the method was not estimated. The results indicate that one might as well use analytic bending equation on a simple bending failure problem.

Figure 3.1b shows that the NLFEA load capacity surface using the UNP method has some local inconsistencies. They seem to happen for stronger material parameters. All the capacities are taken from converged load steps. At the same time, UNP gets several non-converged steps for even stronger materials. One reason for this, could be the steel strength-dependent hardening modulus. Another explanation could be due to the fixed failure definition used during post-processing. Eurocode 2 and the parabolic concrete model states that the strain for maximum concrete compressive strength increases with the concrete strength. Therefore, using a fixed strain to define failure is very conservative for stronger concrete. This will affect the NLFEA LSFEs and can be one of the reasons for the low NLFEA βs for a load of 60 kN. It is therefore important to note that the method for NLFEA LSFEs is only applicable for a limited range of the stochastic variables. The exact range is not determined in this thesis.

For reliability methods using NLFEA there is a fine balance between applicability, feasibility and accuracy. Different structures have different failure modes. To run a reliability analysis on complex structures, the method for NLFEA LSFEs needs to be applicable for several failure modes. It is therefore important that the method for NLFEA LSFEs manages to account for all failure modes, or that they are known beforehand. Some form of post-processing can help the method be applicable for several failure modes, but ultimately it is the NLFEA solution strategy which limits the number of detected failure modes. A NLFEA solution strategy that is applicable for bending failure is not necessarily applicable for other failure modes, e.g., shear failure. The results shown in Appendix A clearly show that the solution strategy is not applicable for shear failure, but models bending failure with adequate accuracy and feasibility when post-processing is applied. To be applicable for shear failure, or other failure modes, the feasibility or accuracy of the solution strategy are subject to change. A different solution strategy could change the balancing between applicability, feasibility and accuracy.

4.2 RSM-FORM

When comparing the NFLEA and analytic RSM-FORM reliability indexes for the 5.0 m beam, as seen in Table 3.1, these are very similar for loads between 40-50 kN, but deviate some for 55 and 60 kN. One reason for the difference in β for higher loads, could be that NLFEA LSFEs seem to have larger discrepancies compared to the analytic LSFEs for higher material strengths. Another reason for the larger discrepancies for higher loads, can be the closeness of the center in the joint PDF. A slight difference in the FORM approximations will slice the volume differently, which will influence the reliability result greater when the design points are closer to the median values. This can be visualized in Figure 3.5, where the design point for 60 kN is located nearer the median values.

Although βs are similar when comparing the analytic and NLFEA RSM-FORM, the influence factors and thus also the design points, show some small differences. The concrete has overall lower influence with NLFEA. This could be explained by the difference in

concrete material model between NLFEA and analytic LSFEs.

The side study using concrete non-in-situ strength, rather than $f_{c,situ}$, highlights the importance of choosing a proper starting point for NLFEA RSM-FORM. A load of 40 kN was applied, and the RSM-FORM started in the median values, $f_c = 42.52$ MPa, $f_{sy} = 560$ MPa. With this starting point, FORM did not converge. This could be due to the method for NLFEA LSFEs not yielding consistent capacities for high material strengths. Based on results from the in-situ analysis, a new starting point was chosen near what was expected to be the design point. Now, RSM-FORM converged after two RSM iterations. Another interesting feature of this RSM-FORM analysis, as seen in Figure 3.6b, is that the final RS approximation curves the other way compared to all the other RS approximations plotted. This is not necessarily wrong, although when the capacities are compared to other results with similar material strengths, the capacities here seem somewhat underestimated. This might be due to the strength dependent E_{har}.

Constructing an approximation of the real RS is a vital part of the RSM-FORM method. Output from the LSFEs influence the accuracy of the approximated RS, but is not an error introduced by the construction scheme itself. Errors relating to RSM are mainly due to the polynomial degree and the f-factors. A comprehensive optimization of the construction procedure with respect to f-factors and polynomial degree is beyond the scope of this study.

Firstly, a second order polynomial was chosen without mixed terms. Higher polynomial degree or mixed terms could increase the accuracy, but then the number of analyses required to build the RS will increase. This is especially relevant for NLFEA as a single analysis is time consuming. Further, higher order polynomials can lead to irregular behavior away from the sample points [3]. Results herein show that creating an accurate RS becomes more difficult as the degree of non-linearity increases, i.e., when several failure modes intersect. Figure 3.5a shows the approximated RS together with the actual LSF. Since only the moment LSF governs the failure domain, the construction procedure of RS applied in this study manages to accurately represent the real LSF. Now, for the 2.3 m beam, two LSFs intersect and that complicates the construction of RS, as seen in Figure

3.8b. This might explain why errors related to the 2.3 m beam are greater than for the 1.5 m and 5.0 m beam, as seen in Table 3.2.

Secondly, f-factors are equally important in constructing the RS approximation as they define the size of the region for where the approximation is most accurate. If the f-factors are too large, then important information might get lost between sample points. On the other hand, choosing too small values provide accuracy in a limited region of the LSF. In NLFEA small f-factors are not recommended unless the FE model is accurate enough to account for small changes in input values. In Figures 3.8a and 3.8b it is clearly observed how an f-factor of 3.0 is large enough to capture the moment LSF, while for an f-factor of 1.0 only the shear LSF governs the failure region. For an f-factor of 1.0, the FORM linearization of the RS coincides with the shear LSF resulting in a failure region solely defined by the shear LSF. Thus, the additional failure region due to moment is not included, and β should be overestimated. Figure 3.9 shows how β changes with different f-factors. Notice how a large f-factor, which includes moment LSF more accurately, still overestimates β and even more so than if the f-factor only covers the shear LSF. This highlights the importance of choosing an adequate f-factor and the difficulty in doing so when several failure modes are present. Intuitively, an f-factor accounting for both failure modes seems like the best choice, but the 2.3 m beam indicates that this is not necessarily the case.

For the 1.5 m beam failing in shear, one would expect to have negligible β-error compared to the Monte Carlo simulations. This comes from that only the shear part of the LSF governs the failure region, and the FORM linearization is equal to it. The moment LSF does not contribute to the reliability since it is too far away from any significant volume in the joint PDF. However, as seen in Table 3.2 there is still an error in the βs. This difference might be due to the Monte Carlo simulations. Three runs were performed for each load, and the mean was taken as β. Since the sampling sets are made from random values of the PDF of the materials, slightly different sampling sets are produced each time, which yield slightly different βs. If a larger sample was used, and performed more than three times, hopefully this statistical error would go towards zero.

4.3 Latin hypercube sampling

From Table 3.8, βs from NLFEA LHS-fit are generally different from Monte Carlo, but more similar to analytic LHS-fit, except for loads equal to 55 kN and 60 kN. It is important to emphasize that induction of any generalizations from such small samples comes with great statistical uncertainty. However, the results indicate that the differences between Monte Carlo simulations and NLFEA LHS-fit are due to the probabilistic model alone for loads less than 55 kN, and a combined error of NLFEA and the probabilistic model for loads greater than 55 kN. This is due to the imperfect method for NLFEA LSFEs. According to Novák et al. [32], the method of approximating PDFs to response outputs from which failure probabilities are calculated is not very accurate. It seems reasonable that a PDF created from only 50 samples for calculating failure probabilities of magnitudes 10^{-5}, does not yield accurate values. More samples are required to properly account for the tail of the PDF, as indicated by the larger standard deviations on the outskirts shown in Table 3.8. An intuitive remedy is to increase the amount of samples, but that would be infeasible with NLFEA. In order to find out if the error related to the probabilistic model is caused by curve fitting or by the small sample size, larger samples are tested on all three lengths to compare β from curve fitting with βs found from counting. Since NLFEA LHS-fit and analytic LHS-fit are quite similar, the analyses are carried out on analytical LSFs.

LHS-count does not give meaningful answers for small samples. Table 3.9 shows that results from counting improve markedly by increasing the number of samples, while for curve fitting the improvements are minor. This confirms what Novák et al. [32] stated; curve fitting is not very accurate, regardless of the number of samples. However, the results are sufficiently close to the Monte Carlo values, even for only 50 samples, which means that curve fitting PDFs to relatively small samples can serve as a viable first estimation. What is meant by first estimation is that since LHS-fit is simple to understand and provides the full picture of the reliability of the structure, it can be applied first. Reliability levels for different loads can be extracted from the same curve fit and one can get broader insight of the problem before proceeding with more accurate reliability strategies.

Another uncertainty is the choice of distribution for the curve fitting. Schneider [38] states that the resistance tends to a log-normal distribution, hence using a normal PDF can give rise to errors. Table 3.2 shows less accurate results for the 1.5 m beam than for the 5.0 m beam with LHS-fit. Further, Figure 3.11 shows that LHS-fit and LHS-count become very similar after the beam length exceeds the transition zone. These observations indicate that using a normal PDF for beam lengths where shear failure is prevalent yield inaccurate results, while moment load capacity seems to be normally distributed.

An interesting discrepancy in the curve fitting results is depicted graphically in Figure 3.11. The error in β obtained from both calculation methods are constant up to length 2.2 m. This complies with shear failure being dominant in this region and independent of the length of the beam. Beyond this length, the influence of moment failure increases. Hence, one could expect the βs to drop in this region because the failure region is extended by the moment LSF. While this occurs for βs obtained from counting, β from curve fitting increases before it drops. The small increase might be attributed to the introduction of another failure mode. Novak et al. [31] states that curve fitting is not appropriate for highly non-linear LSF. Although Figure 2.21 shows that the combined analytic LSF of shear and moment is not highly non-linear, it might be sufficiently non-linear to cause the inaccuracy.

Curve fitting is not very accurate, but the results herein suggest that the method can serve well as a feasible first estimation. However, for a more complex structure with highly non-linear and intersecting failure modes, the method of curve fitting might become too inaccurate even for first estimation purposes. Several complex LSFs give rise to multiple peaks that complicates the curve fitting procedure.

4.4 Safety formats

Opposed to the global resistance factor method, the resistance obtained from NLFEA in the partial factor method is not divided by a safety factor. Modelling uncertainties are already included in the design values as indicated by (2.32). This can in some cases

lead to very low design values which can result in completely different failure modes and, for statically indeterminate structures, unrealistic load redistribution. However, that is not the case in this study as the beam is statically determined. A drawback for both formats is that the proposed values for modelling uncertainties to be applied are based on simple failure modes and hence limits the range of application of the safety formats [37]. If these formats are applied to more complex structures, without questioning the modelling uncertainties, the results might become inaccurate.

Design resistances calculated according to the global resistance factor method and the partial factor method are 42 433 N and 40 330 N, respectively. The difference between design resistances is large and consequently reliability levels also differ. This may be a result of how uncertainties are incorporated in the two formats. βs corresponding to the design resistances from the safety formats are higher than what to be expected for design values. This does not mean the safety formats yield overly conservative results, rather LHS-fit provides too high resistances. The latter seems to be the case throughout the study as the modelling uncertainties are not implemented in the safety assessment using LHS-fit.

Chapter 5

Conclusion

This report indicates that NLFEA can be used for reliability purposes. A single analysis is time consuming, but RSM-FORM and LHS-fit only require a small number of analyses. However, for the reliability methods to yield accurate results, great efforts must be directed towards the method for NLFEA LSFEs. Results presented show that manual load control yield inconsistent load capacities which further complicates RSM-FORM. Moreover, manual load control is not able to trace the response beyond limit points. This implies that one would have to adjust and optimize the specified load steps until maximum capacity is detected. Doing this for repeated NLFEA is not feasible. The UNP method has two key features that markedly improve the feasibility and accuracy of the reliability assessments. (1) The method is able to trace the response beyond critical points, and (2) it finds the optimal step sizes automatically. However, the UNP method alone still does not suffice, and an additional failure definition implemented during post-processing is pivotal. For both reliability methods, the inaccuracy may increase with the complexity of the LSF. This is due to the inherent shortcomings of the reliability methods, and the fact that creating NLFEA models becomes more challenging. This highlights that errors in NLFEA and errors in the reliability methods are complementary, and must both be mitigated in order to increase the accuracy.

RSM-FORM demands accurate outputs from NLFEA in order to converge. This is because the approximated RS and the following FORM analysis depend on the smoothness of the load capacity surface. The more complex the LSF is, the more difficult it is to create an approximated RS and perform FORM analysis. Large structures are likely to

have intricate failure modes, which could affect the accuracy of the reliability method, and thus making it less applicable.

Results from LHS-fit point out that curve fitting should be used only for preliminary reliability analysis. The curve fitting approach seems invariant with respect to sample size, hence a larger sample size would not increase the accuracy. Further, the accuracy of LHS-fit is dependent on the choice of PDF. Large structures can have a complex LSF that might make the process of curve fitting difficult, and thus affecting the applicability.

In terms of feasibility, RSM-FORM normally requires 10-25 LSFEs for one β, while LHS-fit with 50 LSFEs provides the whole spectrum, meaning that βs for different loads are calculated from the same curve fit. RSM-FORM is more accurate but also requires more from the user as the concept of LHS-fit is simpler to grasp. Further, RSM-FORM seems to overestimate β, while LHS-fit generally provides conservative βs.

It is important to emphasize that the results presented in this report do not necessarily reflect the accuracy or the feasibility of the reliability methods in a general sense. Results indicate that RSM-FORM has good feasibility and accuracy, but struggles with applicability for several failure modes. LHS-fit has good feasibility, but the accuracy and applicability seem to depend on the chosen PDF. Further, despite an optimal choice of PDF, the accuracy may still not be satisfactory. LHS-count has applicability and accuracy comparable to Monte Carlo, but with greater feasibility. However, the feasibility is still low in combination with NLFEA.

Chapter 6

Further research

During the research and discussions, topics arose that could be interesting for further research. In this chapter, the most interesting recommendations are presented.

First of all, it is important to keep in mind that this will hopefully be applied to structural engineering in the foreseeable future. To be applicable for large concrete structures exhibiting several failure modes and a complex non-linear behavior, FORM might not be the best reliability method. Other methods for reliability calculations that can be applicable include SORM and system reliability methods, e.g., the Branch-and-Bound method [43].

In addition to a different reliability method, another RS approximation technique could be helpful. Allaix and Carbone [3] presents an improvement on how to construct the RS. For a RS that is accurate in a larger area than just in the design point, one can run Monte Carlo with LHS and importance sampling.

In this study, only two material parameters were considered stochastic variables. It would be interesting to use more stochastic variables, and see how this affects the reliability. However, due to feasibility, a wise choice regarding the number of variables must be done. A suitable next choice could be to include the load as a stochastic variable.

A lot of information was discarded from NLFEA, e.g., cracks, deflections, that could have been used in safety assessments focusing on service limit state. This information is valu-

able in design of concrete structures and should be evaluated rather than just neglected.

The general use of reliability analyses for large concrete structures using NLFEA requires a very robust solution strategy. As seen in this report, the method used was not able to account for shear failure. Therefore, creating a general NLFEA method is a complicated task that requires further study.

Appendix A

Optimization of the method for NLFEA LSFEs

In this appendix, the methods are summarized, the results are presented and the last section provides a discussion and conclusion on the results.

A.1 Method

To get accurate results in a feasible way, an optimization of the method for NLFEA LSFEs was needed. This optimization was done for the 5.0 m beam with the same FE model and material models as described in Section 2.5. Since convergence in RSM-FORM requires a certain degree of consistency in the method for NLFEA LSFEs, RSM-FORM analyses were performed to test feasibility and accuracy. When inconsistent load capacities occur *within* one RSM iteration, the RS approximation becomes inaccurate. FORM might still find the next estimation of the design point, but this estimation can be far away from the real design point, and RSM-FORM does not converge. Inconsistent load capacities *between* RSM iterations only give slow convergence. RSM-FORM is therefore used as a simple tool to check the level of consistency. To test the accuracy of the method for NLFEA LSFEs, analyses can be compared to experimental results. Since no experiment was conducted, these values were compared to the results using the modified analytic formulas. Feasibility was assessed by comparing the computational time. To test the applicability of the method for NLFEA LSFEs, the beam length was changed to 1.5 m, keeping other factors constant. The f-factor for RSM was set to 3.0 for all analyses.

Two NLFEA analysis procedures were tested; manual load control with modified N-R iterations, hereby referred to as manual load control, and updated normal plane arc-length method with regular N-R iterations, hereby referred to as UNP. The two analysis procedures are summarized in Table A.1 and A.2, respectively. Automatic load control and Quasi-Newton were also briefly tested, but showed little promise and were quickly discarded. These results are not included.

Table A.1: Manual load control properties

Property	**Value**
Load steps	0.1(3) 0.01(5) 0.002(150)
Iterative solver	Modified N-R
Max iterations	1000
Line search	No
Convergence norm (either):	
Energy	< 0.001
Force	< 0.01
No convergence	Continue
Abort criterion	> 10000 for both

Table A.2: UNP properties

Property	**Value**
Load steps	0.1(100)
Arc-length method	Updated Normal Plane
Control type	Regular (no control set)
Unloading determination	Sign change
Iterative solver	Regular N-R
Max iterations	100
Line search:	
Lower bound	0.1
Upper bound	1
Maximum number of searches	5
Energy criterion [Psi]	0.8
Regula Falsi interval Delta eta	0.1
Convergence norm (either):	
Energy	< 0.001
Force	< 0.01
No convergence	Continue
Abort criterion	> 10000 for both

Three different failure definitions, defined in Table A.3, were applied in the post-processing to both analysis procedures. Thus, six different methods for NLFEA LSFEs were compared.

Table A.3: Failure definitions for the 5.0 m beam

Failure definition	**Failure**
Max load	The maximum converged load the NLFEA software finds.
Concrete strength dependent strain failure (CSD strain failure)	Failure occurs when the principal compressive concrete strain, ϵ_c, in either of the integration points in the element group *Crush*, seen in Figure 2.19, exceeds the strain for maximum compressive strength of the concrete defined in (2.13). The last step before this strain is exceeded is taken as the capacity.
Fixed strain failure	The strain, ϵ_c, in the integration points in *Crush*, seen in Figure 2.19, limits the region where the max converged load is searched for. The strain limit was set to 1.8‰, which is ϵ_{c1} for the weakest concrete in Eurocode 2.

The reinforcement stresses, σ_s, in the integration points in *Reinf*, seen in Figure 2.19, were also monitored to check if the reinforcement had yielded.

A.2 Results

The following tables present results from various RSM iterations. The first row corresponds to the last estimated design point, while the four other are sample points for the RSM procedure. A consistent result means that higher material parameters yield higher capacities. Interesting results are marked with **bold text**.

A.2.1 5.0 m beam

Firstly, the results for the manual load control with the three failure definitions are presented. Manual load control gives highly inconsistent LSFEs for all failure definitions. Secondly, the UNP method with the three failure definitions are presented. Using max load as failure definition gives inconsistent LSFEs, while the other failure definitions improve the consistency.

Manual load control

A typical load-deflection plot using manual load control for the 5.0 m beam is shown in figure A.1.

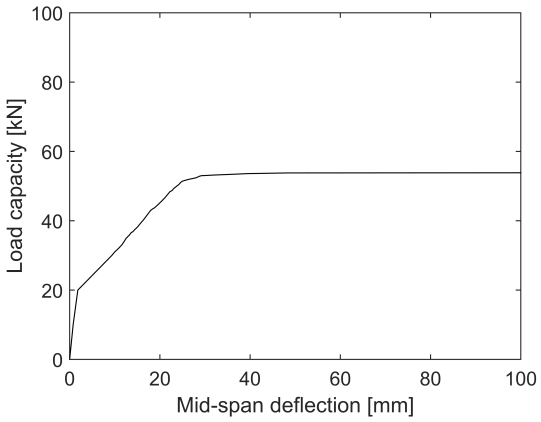

Figure A.1: Load-deflection curve for $f_{c,situ} = 29.1987$ MPa and $f_{sy} = 560.0000$ MPa using manual load control

The result from the first RSM iteration using manual load control for the 5.0 m beam with a load of 40 kN with the three failure definitions are shown in Table A.4, A.5 and A.6. Note that for all failure definitions, material combination no. 1 and no. 3 are inconsistent.

Table A.4 shows two problems with manual load control with max load as the failure definition: (1) convergence in the NLFEA software was found for extremely high concrete strains and mid-span deflections, and (2) the load capacities are inconsistent.

Table A.4: Results for RSM iteration 1 for 40 kN using manual load control with max load as the failure definition

$f_{c,situ}$ [MPa]	f_{sy} [MPa]	Load capacity [N]	Deflection [mm]	ϵ_c [-]	σ_s [MPa]
29.1987	**560.0000**	**54 200**	**14840.0**	**-69.6600**	**700.0**
19.2991	560.0000	48 400	1378.0	-5.9940	700.0
44.1763	**560.0000**	**53 200**	**270.6**	**-0.2470**	**638.0**
29.1987	489.8000	46 400	$5.97 \cdot 10^{11}$	$-2.15 \cdot 10^{9}$	612.3
29.1987	**630.2000**	**51 000**	**67.8**	**-0.0822**	**638.9**

In an attempt to fix these unrealistic large strains and deflections, the CSD strain failure definition was applied. Table A.5 shows the results with this failure definition. The response is more realistic, but the load capacities are still inconsistent.

Table A.5: Results for RSM iteration 1 for 40 kN using manual load control with CSD strain failure as the failure definition

$f_{c,situ}$ [MPa]	f_{sy} [MPa]	Load capacity [N]	Deflection [mm]	ϵ_c [-]	σ_s [MPa]
29.1987	**560.0000**	**53 200**	**32.2**	**-0.0015**	**561.9**
19.2991	560.0000	39 800	17.7	-0.0012	425.2
44.1763	**560.0000**	**52 600**	**58.7**	**-0.0014**	**569.2**
29.1987	489.8000	45 000	31.5	-0.0015	494.9
29.1987	**630.2000**	**49 000**	**32.1**	**-0.0015**	**584.0**

In a final attempt to fix the inconsistencies, the third failure definition, fixed strain failure, was applied. Table A.6 shows the results with this failure definition. The inconsistent load capacities are still prevalent.

Table A.6: Results for RSM iteration 1 for 40 kN using manual load control with fixed strain failure as the failure definition

$f_{c,situ}$ [MPa]	f_{sy} [MPa]	Load capacity [N]	Deflection [mm]	ϵ_c [-]	σ_s [MPa]
29.1987	**560.0000**	**53 200**	**32.2**	**-0.0015**	**561.9**
19.2991	560.0000	40 400	19.0	-0.0017	438.7
44.1763	**560.0000**	**52 600**	**58.7**	**-0.0014**	**569.2**
29.1987	489.8000	45 000	31.5	-0.0015	494.9
29.1987	**630.2000**	**49 400**	**32.8**	**-0.0017**	**589.2**

To visualize the inconsistencies for the manual load control with fixed strain failure definition, the load capacity surface is shown in Figure A.2. Some plots for specific material strengths were made to better show the inconsistencies. The plots show another problem with manual load control: slightly different material strengths yield the same load capacities due to the discrete load steps for all material combinations.

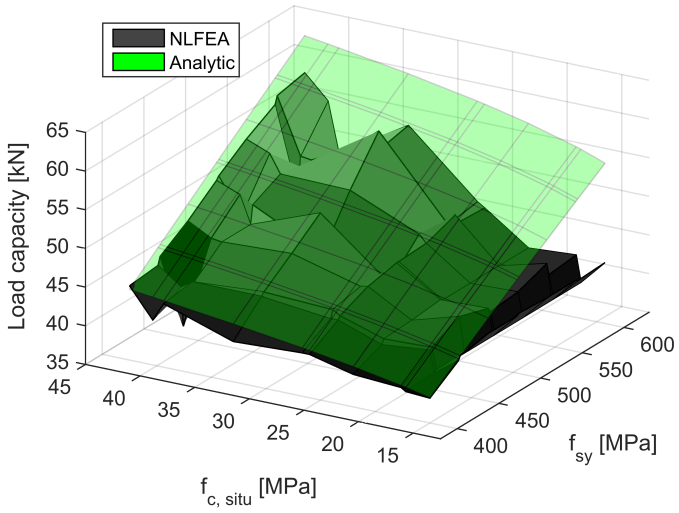

(a) Load capacity surface plot

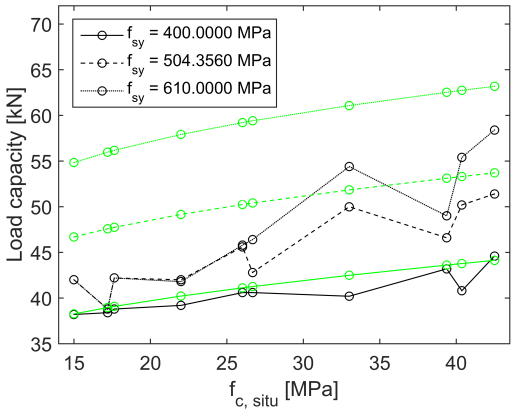

(b) Load capacities for varying $f_{c,situ}$

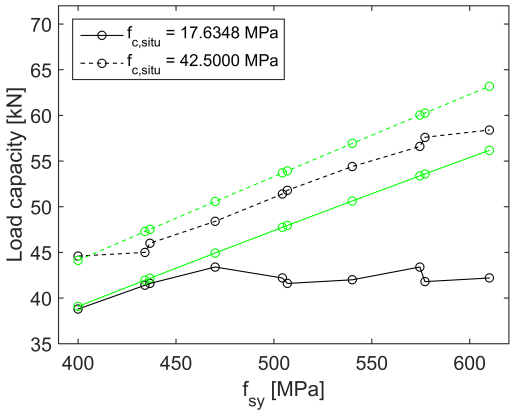

(c) Load capacities for varying f_{sy}

Figure A.2: Load capacities of the 5.0 m beam using manual load control with the fixed strain failure definition

Updated normal plane arc-length method

To overcome the shortcomings found for manual load control, the UNP method was tested. A typical load-deflection plot with the arc-length method is shown in Figure A.3

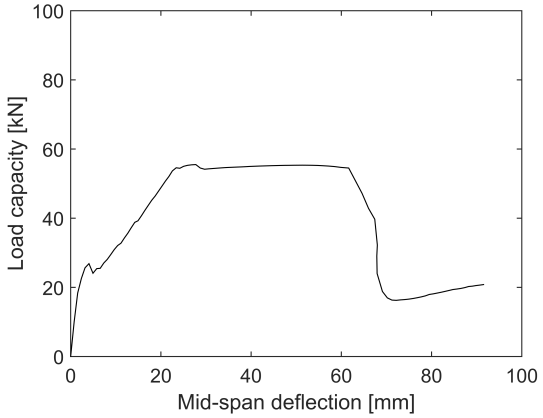

Figure A.3: Load-deflection curve for $f_{c,situ} = 29.1987$ MPa and $f_{sy} = 560.0000$ MPa using the UNP method

Table A.7 shows the results using the UNP method with max load as the failure definition for RSM iteration 2 for a load of 40 kN. This method yields relatively large concrete strains and deflections, in addition to the capacities being inconsistent. RSM-FORM converged for a load of 45 kN, but did not converge for other loads.

Table A.7: Results for RSM iteration 2 for 40 kN using UNP with max load as the failure definition

$f_{c,situ}$ [MPa]	f_{sy} [MPa]	Load capacity [N]	Deflection [mm]	ϵ_c [-]	σ_s [MPa]
18.0669	**410.6832**	**42 580**	**72.3**	**-0.0078**	**444.8**
11.9415	410.6832	39 060	17.8	-0.0012	414.1
27.3344	**410.6832**	**42 250**	**26.3**	**-0.0017**	**426.7**
18.0669	340.4832	36 570	55.0	-0.0056	367.0
18.0669	480.8832	48 530	64.8	-0.0078	512.7

The different concrete strains at the load capacities gave the idea of limiting the allowed strain. Once again, the CSD strain failure definition was tested in an attempt to get RSM-FORM convergence for several loads. As shown in Table A.8, this failure definition is conservative compared to the max load failure definition for low concrete strengths.

Table A.8: Results for RSM iteration 2 for 39 kN using UNP with CSD strain failure as the failure definition

$f_{c,situ}$ [MPa]	f_{sy} [MPa]	Load capacity [N]	Deflection [mm]	ϵ_c [-]	σ_s [MPa]
16.9163	437.4890	42 280	17.8	-0.0009	439.1
11.1810	**437.4890**	**35 460**	**14.9**	**-0.0008**	**361.2**
25.5937	437.4890	43 820	21.1	-0.0013	449.4
16.9163	367.2890	36 490	15.2	-0.0009	371.8
16.9163	507.6890	47 130	20.5	-0.0011	502.3

To remedy the conservative load capacity of the weak concrete, the fixed strain failure definition was applied to the UNP method. This gave no inconsistencies within RSM iterations, and RSM-FORM converged for two to four RSM iterations for loads of 40, 45, 55 and 60 kN, but needed eight RSM iterations for a load of 50 kN. RSM-FORM failed to converge for 65 kN due to shortcomings of the NLFEA solution strategy. The results from 65 kN is seen in Table A.9. Here, combination no. 5 does not have a converged capacity. This solution strategy does not seem to be applicable for high reinforcement strengths.

Table A.9: Results for RSM iteration 2 for 65 kN using the UNP method with fixed strain failure definition

$f_{c,situ}$ [MPa]	f_{sy} [MPa]	Load capacity [N]	Deflection [mm]	ϵ_c [-]	σ_s [MPa]
34.8700	**658.9307**	**63 420**	**32.3**	**-0.0012**	**659.0**
23.0476	658.9307	61 980	28.6	-0.0015	659.4
52.7568	658.9307	66 210	44.4	-0.0011	665.3
34.8700	588.7307	60 100	53.7	-0.0016	610.9
34.8700	**729.1307**	**61 390**	**32.9**	**-0.0012**	**628.8**

For a load of 50 kN, the NLFEA results were consistent within each RSM iteration. However, inconsistencies between RSM iterations occurred. Small increases in both material strengths gave lower capacity. This is seen in Table A.10. RSM-FORM converged, but

more iterations were needed than for other RSM-FORM analyses.

Table A.10: Results for material combination no. 2 in RSM iteration 5 and 6 for 50 kN using the UNP method with fixed strain failure definition

RSM iteration	$f_{c,situ}$	f_{sy}	**Load capacity**	**Deflection**	ϵ_c	σ_s
#	**[MPa]**	**[MPa]**	**[N]**	**[mm]**	**[-]**	**[MPa]**
5	17.2007	504.3560	48 390	22.3	-0.0013	510.0
6	17.6348	506.9042	48 300	21.1	-0.0011	507.9

The first RSM iteration for 40 kN using the UNP method with fixed strain failure definition is shown in Table A.11. This shows consistency, as opposed to Table A.4, and implies the importance of a proper method for NLFEA LSFEs.

Table A.11: Results for RSM iteration 1 for 40 kN using the UNP method with fixed strain failure definition

$f_{c,situ}$	f_{sy}	**Load capacity**	**Deflection**	ϵ_c	σ_s
[MPa]	**[MPa]**	**[N]**	**[mm]**	**[-]**	**[MPa]**
29.1987	560.0000	55 510	27.7	-0.0016	572.1
19.2991	560.0000	52 130	23.2	-0.0017	560.4
44.1763	560.0000	57 260	42.2	-0.0018	592.0
29.1987	489.8000	49 390	25.8	-0.0015	502.0
29.1987	630.2000	61 580	29.8	-0.0017	639.7

As seen on the load capacity surface plot using the UNP method with fixed strain failure definition in Figure A.4, the accuracy is improved. However, this method still shows some inconsistencies. These are smaller than those of manual load control, but can still lead to slow convergence.

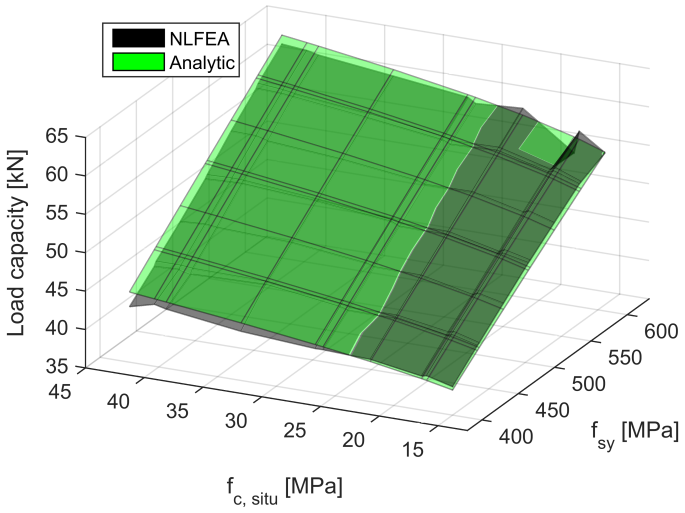

(a) Load capacity surface plot

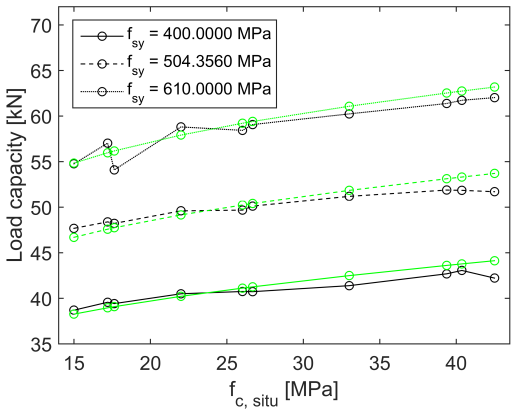

(b) Load capacities for varying $f_{c,situ}$

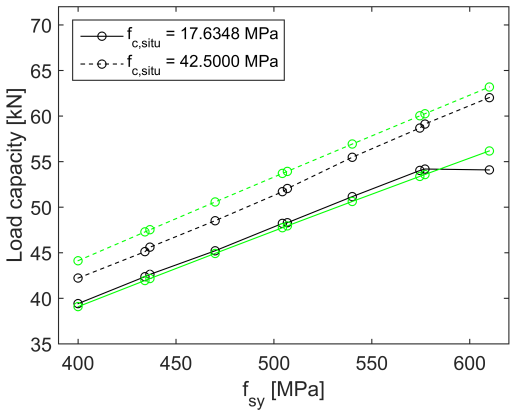

(c) Load capacities for varying f_{sy}

Figure A.4: Load capacities of the 5.0 m beam using the UNP method with fixed strain failure definition

Different computers were used when analysing the results. It was noticed a slight different in the output from Diana. Table A.12 shows the difference for RSM iteration 1 with a load of 40 kN.

Table A.12: Results for RSM iteration 1 for 40 kN using the UNP method with fixed strain failure definition for a different computer

$f_{c,situ}$ [MPa]	f_{sy} [MPa]	Load capacity [N]	Deflection [mm]	ϵ_c [-]	σ_s [MPa]
29.1987	560.0000	55 470	27.8	-0.0015	572.1
19.2991	560.0000	52 220	23.2	-0.0017	560.4
44.1763	560.0000	56 900	39.0	-0.0018	592.0
29.1987	489.8000	49 410	25.8	-0.0015	502.0
29.1987	630.2000	61 530	28.9	-0.0013	639.7

A.2.2 1.5 m beam

Load-deflection plots for three analysis in the first RSM iteration are shown in Figure A.5. Since the longitudinal reinforcement did not contribute to the capacity, only the plots for varying $f_{c,situ}$ are shown. Three different failure definitions were applied to the 1.5 m beam; (1) max (converged) load, (2) limiting the deflection to 0.3 mm, and (3) using the first peak in the load deflection plots. All failure definitions underestimated the load capacity when compared to the analytic equation. Only the results with max load as the failure definition are presented.

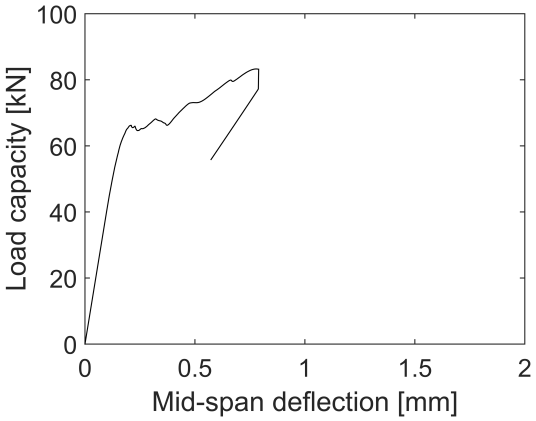

(a) $f_{c,situ} = 29.1987$ MPa and $f_{sy} = 560.0000$ MPa

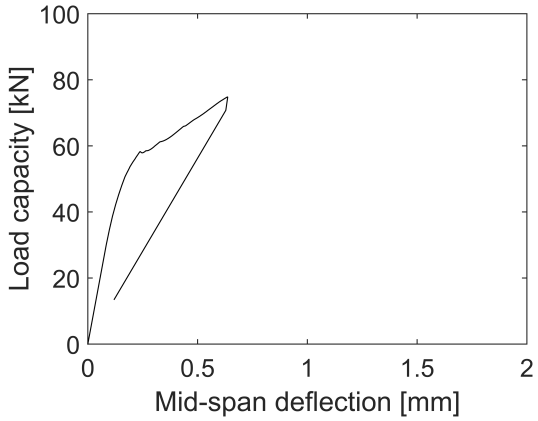

(b) $f_{c,situ} = 19.2991$ MPa and $f_{sy} = 560.0000$ MPa

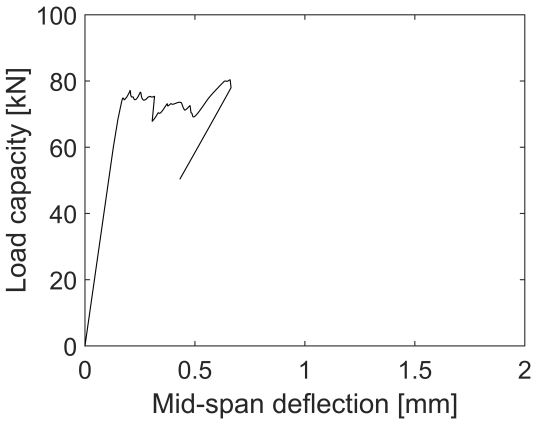

(c) $f_{c,situ} = 44.1763$ MPa and $f_{sy} = 560.0000$ MPa

Figure A.5: Load-deflection curves for the UNP method using max load as the failure definition

The results from the first RSM iteration for 73 kN load using max load as the failure criterion is shown in Table A.13. It is evident that the longitudinal reinforcement does not contribute for the shorter beam, as material combination no. 1, 4 and 5 yield the same capacity. Max load shows inconsistencies with combinations no. 1 and 3.

Table A.13: Results for RSM iteration 1 with 85 kN using UNP with max load as the failure definition

$f_{c,situ}$ [MPa]	f_{sy} [MPa]	**Load capacity** [N]	**Deflection** [mm]
29.1987	**560.0000**	**83 280**	**0.78**
19.2991	560.0000	74 830	0.64
44.1763	**560.0000**	**80 410**	**0.66**
29.1987	489.8000	83 280	0.78
29.1987	630.2000	83 280	0.78

A.3 Discussion and conclusion

The greatest obstacle using NLFEA for large structure reliability analyses is to balance accuracy and feasibility. Having to manually check all outputs is unfeasible, and the method for NLFEA LSFEs should be able to detect failure somewhat automatically. The same solution strategy should also be used for all the analyses. With that said, manual load control falls short of the UNP method in regards to both feasibility and accuracy.

As seen in Figure A.2, manual load control gives low accuracy compared to the analytic formulas for the 5.0 m beam for all failure definitions. It seems the manual load control is simply not able to surpass the limit points for concrete cracking, even with specifying the analysis procedure to continue for no convergence in the iterative solver. At the same time, manual load control gives discrete capacities. The problem could be remedied in two ways: (1) changing the load incrementation between analyses or (2) automatic load control. Having to change the load incrementation manually is simply unfeasible for repeated NLFEAs. The brief testing on automatic load control encountered problems. More optimization could be done to improve load control, but the UNP method showed more promise.

As shown in Figure A.4, the UNP method with fixed strain failure seems very accurate compared to the analytic formulas for the 5.0 m beam. The other failure definitions yield

less accurate results. This highlights that proper post-processing can improve the accuracy of the method. Arc-length methods have automatic incrementation, hence the UNP method can be applied to several material parameters without major modifications. This makes it more feasible for design purposes. Moreover, the computational time is lower than the manual load control method. The UNP method seems like the better choice when analyzing bending problems with NLFEA.

Compared to analytic load capacities, the UNP method give low load capacities for the 1.5 m beam. Other failure definitions gave consistency, but the low capacities cannot be fixed with post-processing. The solution strategy with the UNP method is not applicable for shear flexure failure. Modifications to the solution strategy are needed to properly model this failure mode.

One important thing to note is that the UNP method gave different load capacities between several computers. The reason is unknown. This means that the load capacity found with the UNP method can be treated a stochastic variable that needs to be taken into account for a full probabilistic reliability analysis.

Appendix B

Analytic capacity equations

The analytic LSF in this study was expressed by either bending moment or shear flexure failure. Both capacity equations originated from Eurocode 2 [2], and are modified to exclude the code-provided safety.

B.1 Moment capacity

To derive the moment part of the LSF, moment capacity must be calculated. This is done using strain and stress assumptions along with force and moment equilibrium. Figure B.1 illustrates a rectangular cross-section of the assessed beam.

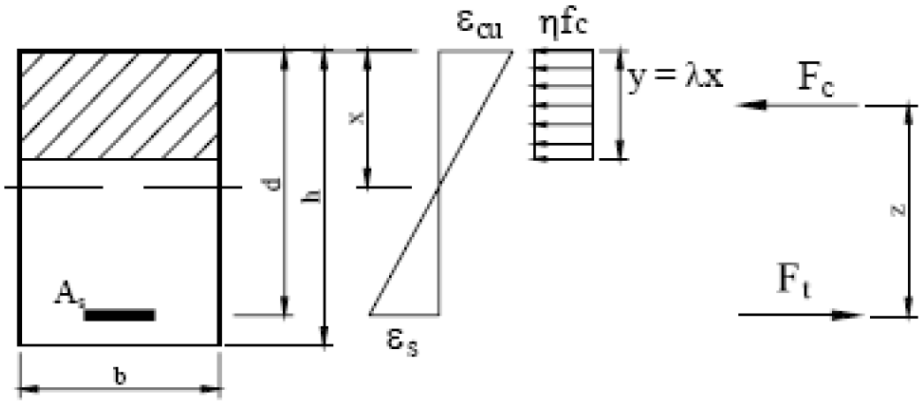

Figure B.1: Beam section, material strains, stresses and forces [21]

As illustrated strains were assumed linear over the height, with ϵ_{cu} at the top. Effective concrete compressive stress is assumed to be the product of a factor, $\eta = 1.0$, and maximum strength, f_c, which is set to $f_{c,situ}$. The product is constant over an effective

compressive zone height expressed by

$$y = \lambda x \tag{B.1}$$

Where x represents the compressive height, and λ a reduction factor of 0.8. Force equilibrium gives

$$F_c = F_t \tag{B.2}$$

Where F_c is the compressive force in the concrete and F_s is the tensile force in the reinforcement. These can be expanded to

$$F_c = \eta\lambda\omega b d f_{c,situ} \qquad \text{and} \qquad F_t = E_{s,mod}\epsilon_s A_s \tag{B.3}$$

where b is the cross-sectional width, d is the effective depth, ϵ_s is the reinforcement strain, A_s is the reinforcement area, ω is x/d in Figure B.1, and $E_{s,mod}$ is a modification of steel's Youngs Modulus due to the use of a bi-linear stress-strain curve, expressed by

$$E_{s,mod} = \frac{f_{sy} + E_{har}(\epsilon_s - \epsilon_{sy})}{\epsilon_s} \tag{B.4}$$

where E_{har} is the hardening modulus attained from (2.16).

According to Sørensen [40], there are two failure criteria for beam failing in bending: By compressive fracture of the concrete, or when the tensile strain in the reinforcement reaches an ultimate value. In the case of steel reaching its ultimate strain, ϵ_{su}, (B.2) and (B.3) is combined to calculate ω. In the case of steel not reaching its ultimate strain, strain linearity gives an expression for ω by

$$\omega = \frac{\epsilon_{cu}}{\epsilon_s + \epsilon_{cu}} \tag{B.5}$$

where ϵ_s is solved with iterative methods using the following second order equation:

$$(E_{s,mod}\rho)\epsilon_s^2 + (E_{s,mod}\rho\epsilon_{cu})\epsilon_s - \eta\lambda\epsilon_{cu}f_{c,situ} = 0 \tag{B.6}$$

where $\rho = \frac{A_s}{bd}$ is the reinforcement ratio. Once ω is known, the moment capacity can be found by moment equilibrium of the cross-section:

$$M_r = F_c(0.2 + \frac{1}{2}0.8)\omega d + F_t(1-\omega)d \tag{B.7}$$

B.2 Shear flexure capacity

The equation for calculating the shear flexure capacity of the concrete is empirical. This can be found in Eurocode 2 on the following form:

$$V_r = Ck(100\rho_l f_c)^{1/3} b_w d \tag{B.8}$$

where C accounts for several dependencies, $k = 1 + \sqrt{\frac{200}{d}}$ is the scale factor, ρ_l denotes the longitudinal reinforcement ratio, f_c is the concrete cylinder strength in MPa, b_w is the minimum beam width in mm, and d is the effective depth in mm. One of the dependencies that the C-factor accounts for is concrete strength. From the Eurocode 2 Commentary [21] and *fib* Bulletin 2 [9], a sample of shear beam capacities were used to calculate the C-factor dependencies, as illustrated in Figure B.2.

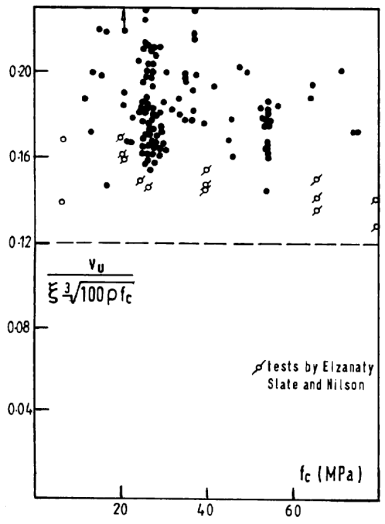

Figure B.2: C-factor of a shear beam sample dependent upon f_c variable [21]

The C-factor is on the Y-axis, with a dotted line representing the Eurocode 2 design value $C = 0.12$ [2]. The unfilled annotations signify a set of special cases which may not have been included in the sample calculations. Assessing standard deviations and median value when assuming normal and log-normal distribution of C, the distribution type is found to be negligible within 1%. Median values of cylinder strength C-factor for total and partial sample is found to be 0.178 and 0.183, respectively.

Due to the dependencies of C, the shear capacity will have a PDF. The median capacity can be defined as the capacity corresponding to 0.5 on its cumulative distribution function.

To achieve a median shear flexure capacity and also account for $f_{c,situ}$, a new value for C is needed. The axes on Figure B.2 are transformed from using f_c to $f_{c,situ}$ The entire transformed sample is illustrated in Figure B.3

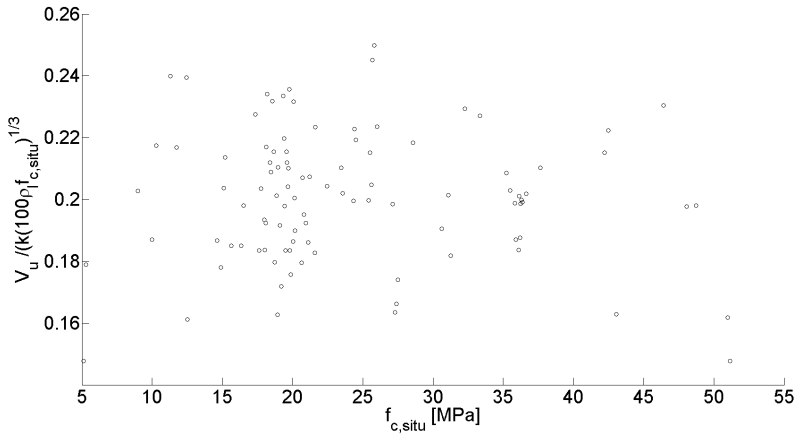

Figure B.3: C-factor of a shear beam sample dependent upon $f_{c,situ}$. The total population from Figure B.2 is included [9]

The new population is also found to give negligible differences whether normal or log-normal distribution is assumed. Median values of the new C-factor for a total and partial sample is found to be 0.200 and 0.205, respectively. The new C-factor is set to 0.20. The median shear flexure capacity, dependent upon $f_{c,situ}$, can now be expressed as

$$V_r = 0.20k(100\rho_l f_{c,situ})^{1/3} b_w d \tag{B.9}$$

Appendix C

Transformation to standard normal space

A standard normally distributed variable has mean $\mu = 0$ and variance $\sigma = 1$, denoted N(0,1). A normally distributed variable is typically denoted N(μ,σ). To transform a normally distributed variable, x_n into a standard normally distributed variable u, the mean, μ_x, and variance, σ_x, must be known. Each number, x_n, in the population is transformed by

$$u = \frac{x_n - \mu_x}{\sigma_x} \tag{C.1}$$

A log-normally distributed variable can be denoted logN(μ,σ). In the case of a log-normally distributed variable, x_{ln}, first this has to be transformed to a normally distributed variable, x_n. This can be done by

$$x_n = ln(x_{ln}) \tag{C.2}$$

Then, the transformation into standard normal space can be performed by (C.1).

Bibliography

[1] *Eurocode 0: Basis of Structural Design.* Standard Norge, 2004.

[2] *Eurocode 2: Design of concrete structures - Part 1-1: General rules and rules for buildings.* Standard Norge, 2004.

[3] D. L. Allaix and V. I. Carbone. An Improvement of the Response Surface Method. *Structural Safety*, 33:165–172, 2011.

[4] K Bell. *An engineering approach to FINITE ELEMENT ANALYSIS of linear structural mechanics problems.* Fagbokforlaget, 1st edition, 2014.

[5] B. Belletti, A. de Boer, C. Damoni, and M. A. N. Hendriks. Validating the Guidelines for Nonlinear Finite Element Analysis of Concrete Structures. Technical report, Rijkswaterstaat, Draft version February 2016.

[6] B. Belletti, A. de Boer, P.H. Damoni, C.and Feenstra, M.A.N. Hendriks, and J.A. den Uijl. Guidelines for Nonlinear Finite Element Analysis of Concrete Structures. Technical report, Draft version February 2016.

[7] G.E.P. Box, W.G. Hunter, and J.S. Hunter. *Statistics for Experimenters, An Introduction to Design Data Analysis and Model Building.* John Wiley & Sons, 1978.

[8] C. G. Bucher and U. Bourgund. A Fast and Efficient Response Surface Approach for Structural Reliability Problems. *Structural Safety*, 7:57–66, 1990.

[9] CEB-FIP. Structural Concrete. Bulletin 2: Textbook for Behaviour, Design and Performance Volume 2. Technical report, *fib*, 1999.

[10] CEB-FIP. *fib* Model Code for Concrete Structures 2010 Final draft Volume 1 and 2. Technical report, *fib*, 2012.

[11] V. Cervenka. Global Safety Format for Nonlinear Calculation of Reinforced Concrete. *Beton- und Stahlbetonbau, 103(1): 37-42*, 2008.

[12] R. D. Cook, D. S. Malkus, M. E. Plesha, and R. J. Witt. *Concepts and Applications of Finite Element Analysis*. John Wiley & Sons, Inc., 4th edition, 2002.

[13] K. Dinga, Z. Zhoub, and C. Liua. Latin hypercube sampling used in the calculation of the fracture probability. *Reliability Engineering & System Safety, 59(2), 239-242*, 1998.

[14] O. Ditlevsen. Model uncertainty in structural reliability. *Structural Safety, 1: 73-86*, 1982.

[15] M. Engen, M. A. N. Hendriks, J. Köhler, J. A. Øverli, and E. Åldstedt. A Quantification of the Modelling Uncertainty of Nonlinear Finite Element Analyses of Large Concrete Structures.

[16] P. H. Feenstra. Computational Aspects of Biaxial Stress in Plain and Reinforced Concrete. Technical report, Delft, 1993.

[17] A. Florian. An efficient sampling scheme: Updated Latin Hypercube Sampling. *Probabilistic Engineering Mechanics, 7(2), 123-130*, 1992.

[18] A.M. Hasofer and N.C. Lind. Exact and Invariant Second-Moment Code Format. *Journal of the Engineering Mechanics Division, 100(1)*, 1974.

[19] D. A. Hordijk. Local Approach to Fatigue of Concrete. Technical report, Delft, 1991.

[20] R.L. Iman and W. J. Conover. A distribution-free approach to inducing rank correlation among input variables. *Communications in Statistics - Simulation and Computation, 11(3): 311-334*, 1982.

[21] J.P. Jacobs, editor. *Eurocode 2 Commentary*. European Concrete Platform ASBL, 2008.

[22] JCSS. *JCSS, Probabilistic model code, 12th draft, Joint Committee on Structural Safety, 2001.*

[23] M. Keramat and R. Kielbasa. Modified Latin Hypercube Sampling Monte Carlo (MLHSMC) Estimation for Average Quality Index. *Analog Integrated Circuits and Signal Processing, 19(1)*, 1999.

[24] P.L. Liu and A. Der Kiureghian. Optimization Algorithms for Structural Reliability. *Structural Safety*, 9:161–177, 1991.

[25] J. Manie. Diana User's Manual - Release 10.0, December 2015. URL `https://support.tnodiana.com/manuals/d100/{D}iana.html`.

[26] K. M. Mathisen. Solution Methods for Nonlinear Finite Element Analysis (NLFEA). https://www.sintef.no/globalassets/project/evitameeting/2012/kmm-geilo-2012-lecture-11a.pdf, January 2012.

[27] K. M. Mathisen. Lecture 2: Solution of Nonlinear Equilibrium Equations, 2015a.

[28] K. M. Mathisen. Lecture 3: Adaptive Solution Algorithms, 2015b.

[29] M. D. Mckay, R. J. Beckman, and W. J. Conover. A Comparison of Three Methods for Selecting Values of Input Variables in the Analysis of Output from a Computer Code. *Technometrics, 21(2), 239-245*, 1979.

[30] B. Minasny. Latin Hypercube Sampling, January 2004. URL `http://www.mathworks.com/matlabcentral/fileexchange/4352-latin-hypercube-sampling`.

[31] D. Novak, B. Teply, and Z. Kersner. The role of Latin Hypercube Sampling method in reliability engineering. 1997.

[32] D. Novák, M. Vorechovský, D. Lehký, R. Rusina, R. Pukl, and V. Cervenka. Stochastic nonlinear fracture mechanics finite element analysis of concrete structures. 2005.

[33] A. Olsson, G. Sandberg, and O. Dahlblom. On Latin hypercube sampling for structural reliability analysis. *Structural Safety, 25(1), 47-68*, 2003.

[34] M. Rajabalinejad. *Reliability Methods for Finite Element Models*. PhD thesis, Delft University of Technology, 2009.

[35] G. Sandberg and A. Olsson. Failure sensitivity analysis of engineering structures. *Computers and Structures, 72(4-5), 525-534*, 1999.

[36] H. Schlune, M. Plos, and K. Gylltoft. Safety formats for nonlinear analysis tested on concrete beams subjected to shear forces and bending moments. *Engineering Structures, 33(8), 2350–2356*, 2011.

[37] H. Schlune, M. Plos, and K. Gylltoft. Safety formats for non-linear analysis of concrete structures. *Magazine of Concrete Research, 64(7), 563-574*, 2012.

[38] J. Schneider. *Introduction to Safety and Reliability of Structures*. International Association for Bridge and Structural Engineering, 2006.

[39] R. G. Selby and F. J. Vecchio. *Three-dimensional Constitutive Relations for Reinforced Concrete*. University of Toronto, dept. Civil Engneering, Toronto, Canada„ 1993.

[40] S. I. Sørensen. *Betongkonstruksjoner*. Akademika forlag, 1. edition, 2013.

[41] P. Thoft Christensen and Y. Murotsu. *Application of Structural Systems Reliability Theory*. Springer-Verlag Berlin, Heidelberg, 1986.

[42] F. J. Vecchio and M. P. Collins. Compression Response of Cracked Reinforced Concrete. *J. Str. Eng., ASCE 119*, 1993(12):3590–3610, 1993.

[43] P. H. Waarts. *Structural reliability using Finite Element Analysis - An appraisel of DARS: Directional Adaptive Response surface Sampling*. PhD thesis, Delft University of Technology, 2000.

[44] R. Zhang and S. Mahadevan. Model uncertainty and Bayesian updating in reliability-based inspection. *Structural Safety, 22(2): 145-160*, 2000.